water

MDPI

Article

Modelling of Granular Sediment Transport in Steady Flow over a Mobile Sloped Bed

Jarosław Biegowski [1], Magdalena Pietrzak [2,*], Iwona Radosz [2] and Leszek M. Kaczmarek [2]

[1] Institute of Hydro-Engineering, Polish Academy of Sciences, Kościerska 7, 80-328 Gdansk, Poland; jaroslawbiegowski@ibwpan.gda.pl
[2] Faculty of Civil Engineering, Environmental and Geodetic Sciences, Koszalin University of Technology, Śniadeckich 2, 75-453 Koszalin, Poland; iwona.radosz@tu.koszalin.pl (I.R.); leszek.kaczmarek@tu.koszalin.pl (L.M.K.)
* Correspondence: magdalena.pietrzak@tu.koszalin.pl

Abstract: This paper introduces a three-layer system, proposing a comprehensive model of granular mixture transport over a mobile sloped bed in a steady flow. This system, consisting of the bottom, contact, and upper zones, provides complete, continuous sediment velocity and concentration vertical profiles. The aim of this study is to develop and experimentally verify this model for sediment transport over a bottom locally sloping in line with or opposite the direction of sediment flow. The model considers gravity's effect on sediment transport in the bottom (dense) layer when the component of gravity parallel to the bottom acts together with shear stresses associated with water flow. This is a crucial factor often overlooked in previous studies. This effect causes an increase in velocity in the mobile sublayer of the dense layer and significantly affects the vertical distributions of velocity and concentration above this layer. The proposed shear variation due to the interaction between fractions and an intensive sediment mixing and sorting process over a mobile sloped bed adds to the novelty of our approach. The data sets used for the model's validation cover various conditions, including slopes, grain diameters, densities, and grain mobility conditions, from incipient motion to a fully mobilized bed. This extensive validation process instils confidence in the theoretical description and its applicability to real-world scenarios in the design of hydraulic infrastructure, such as dams, barrages, bridges, and irrigation, and flood control systems.

Keywords: granular mixture; steady flow; sediment transport rate; sediment velocity; sediment concentration; mobile sloped bed

Citation: Biegowski, J.; Pietrzak, M.; Radosz, I.; Kaczmarek, L.M. Modelling of Granular Sediment Transport in Steady Flow over a Mobile Sloped Bed. *Water* **2024**, *16*, 2022. https://doi.org/10.3390/w16142022

Academic Editor: Bommanna Krishnappan

Received: 3 June 2024
Revised: 10 July 2024
Accepted: 11 July 2024
Published: 17 July 2024

1. Introduction

Structures such as dams significantly affect sediment transport conditions in rivers. Challenges arise in particular from the accumulation of sediment above the water level and erosion of the bottom downstream. To alleviate these problems, engineers develop various technical solutions, such as specialized sediment dams, bottom outlets or concrete channels to flush sediment downstream. Sedimentation in water bodies poses challenges not only from an engineering point of view (reduced retention capacity and the need for periodic dredging), but also for ecosystems (accumulation of pollutants, impeded biological self-cleaning, and adverse effects on biota).

In addition to the problems of sedimentation in reservoirs, the construction of dam facilities involves the risk of downstream bed erosion. In order to counteract this, appropriate bottom stabilization measures are used and cascade dams can be built to raise water levels and reduce downstream flow velocities.

Recent research in sediment transport and hydraulic engineering focuses on various aspects of sediment management in rivers and reservoirs as well as the modelling of these processes. The need for sediment management in reservoirs to maintain their retention capacity and functionality is emphasized [1]. Further, the importance of understanding the

critical flow velocities that determine the initiation of sediment transport, both in uplifted form and at the bottom in dragged form, is highlighted [2]. The literature review on modelling erosion and sediment transport reveals the need for continued development of research methods and tools to better understand and manage morphodynamic processes in rivers and reservoirs, which is crucial for the design and maintenance of hydraulic infrastructure in the face of changing environmental conditions. Indeed, there is still no complete mathematical description of sediment transport that would allow reliable prediction over a wide range of hydrodynamic conditions, as pointed out by Berzi and Fraccarollo [3,4].

Key knowledge for engineers and designers includes sediment transport issues, especially over mobile sloped bed. Although engineers often resort to readily available empirical formulas for calculations of sediment transport, over the sloped bed, this approach can lead to errors due to still insufficient advanced theoretical models and appropriate numerical solutions.

Classical formulas for calculating sediment transport, such as the Meyer–Peter and Müller formula [5], are inadequate under conditions of steep bottom slopes as they rely on the critical friction parameter [6], which varies with gradient.

In response to these challenges, authors such as Smart [7], Wong and Parker [8], and Cheng and Chen [9] attempted to modify existing formulas by adjusting the value of the critical Shields parameter for conditions of steep bottom slopes.

Graf and Suszka [10] developed their own empirical formula to adjust parameters for significant bottom slopes. Additionally, the studies of Recking et al. [11] and Parker et al. [12] focus on adjusting the value of critical Shields stress depending on bottom slope, grain diameter, and other factors. However, Maurin et al. [13] emphasize that the bottom slope may not affect only the value of the Shields [6] parameter, but many of the physical processes that accompany it.

Lamb et al. [14] presented a mathematical model based on vertical force equilibrium and a classical description of turbulence, emphasizing that at high bottom slopes, grain movement is more influenced by turbulence than bottom friction. In contrast, the study conducted by Dang et al. [15] focuses on analyzing the effect of changes in the bottom level of mountain rivers on sediment transport using numerical and experimental models. These findings provide new data on the relationship between bottom structure and sediment transport in mountain rivers, taking into account a variety of flow and topography conditions.

A study by the Maritime Research Institute The Netherlands [16] uses experiments in large wave channels to analyze the effect of bottom slope on beach morphological changes and sediment transport during different wave conditions. The results show how varying wave conditions can affect sediment transport processes in coastal zones.

Research by Chinese scientists [17] introduces a new methodology for measuring sediment transport capacity on steep slopes using a specially designed channel. This method allows for more accurate measurements of sediment transport capacity under different slope and flow conditions, which is crucial for modelling erosion on hillsides.

Tan W. and Yuan J. [18–20] described the experiments under sinusoidal oscillatory flows over a sloping bed. They argued that the effects induced by the bed slope on sediment transport may be as important as the effects due to the wave's asymmetry.

Recently, Radosz et al. [21,22] collected measurements on the vertical structure of sediment fluxes during the wave crest and trough phase over the sloped bed. The experimental work included measurements using the particle image method and measurements of sediment transport and granulometric distributions of sediments collected in the traps on both sides of the sloped initial area. The experimental data were compared with theoretical analysis based on a three-layer model of graded sediment transport in wave motion Kaczmarek et al. [23–25] and in steady flow conditions [26–28].

In summary, most authors focus either on modification or development of new formulas and mathematical models that will better describe the behavior of sediments at

steep bottom slopes, with particular attention to the description of flow turbulence and the vertical structure of sediment transport.

The aim of this study is to develop and experimentally verify a three-layer model for the transport and vertical structure of transport and segregation of non-cohesive and granulometrically heterogeneous sediments under steady flow conditions over the sloped bed in an open channel. The model describes the transport of sediment over a bottom locally sloping in line with or opposite to the direction of sediment motion, ranging from zero to slopes close to the value of the angle of internal friction. The proposed theoretical model is validated with many data sets for different slopes, grain diameters, and densities in a wide range of grain mobility conditions for incipient motion to a fully mobilized bed.

2. Materials and Methods

2.1. Theoretical Model Assumptions

Under flow conditions, sediment transport near the bottom occurs as a result of the energy imparted by the fluid in motion via shear stresses, which are a measure of friction against the bottom of fluid elements. Shear stress τ'_* as the causal factor of sediment movement is described by friction velocity as follows:

$$\tau'_* = \rho u'^2_{f*}\,, \tag{1}$$

where ρ—is the water density.

The friction velocity u'_{f*} is an input in modelling. In order to determine this friction velocity u'_{f*} from the experiments, it is proposed to find the friction velocity value from Equation (2) for measured velocity profile:

$$u = \frac{u'_{f*}}{\varkappa} ln \frac{z}{k_s/30}\,, \tag{2}$$

where k_s is the skin roughess assumed $k_s = 2.5d_{50}$, $\varkappa$ is von Karmen constant (assumed as 0.40), and d_{50} is median diameter. The vertical axis is directed upward with the origin $z = {}^{k_s}/_{30}$ at the bottom.

Under open channel flow conditions due to gravitational forces, shear stresses τ'_* are a measure of friction against the bottom of a fluid element of depth h^* (Figure 1):

$$-\tau'_* = \rho g h^* I, \tag{3}$$

where I is the slope of energy line and g is the earth's acceleration.

Under steady-state uniform flow conditions (i.e., where the water depth, cross-sectional area, and water velocity in each channel cross-section are constant), the energy line I is parallel to the bottom slope S (Figure 1), with the following relationships:

$$h^* = hcos\xi,\ I = S = sin\xi. \tag{4}$$

2.2. Three-Layer Transport Structure

Sediment transport varies in nature and is accompanied by different physical processes depending on the distance from the bottom to the free surface of the water. At the bottom, there are high concentrations and lower velocities, and there is an intensive exchange of momentum between sediment grains as a result of their collisions with each other. In the immediate vicinity of the bottom, there is sorting of grains, some of which fall back to the bottom, and the rest are transported in suspension, which occurs up to the free water level.

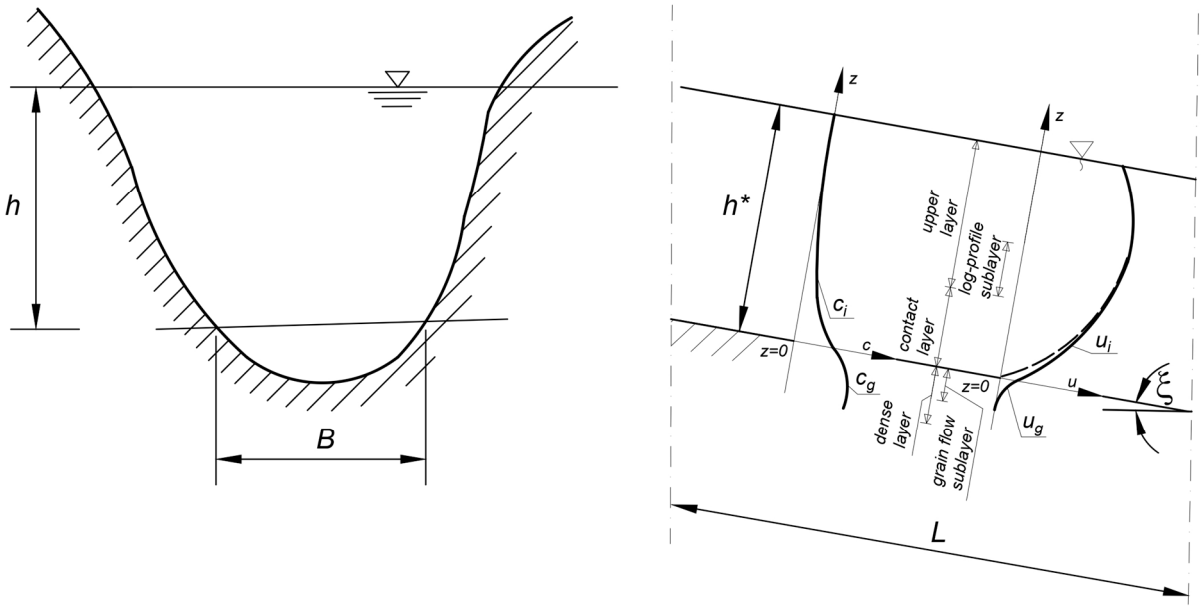

Figure 1. Diagram of steady water flow with a three-layer system of sediment transport in open channels over a strongly sloping bottom; c—sediment concentration; c_i—vertical profile of $i-th$ fraction concentration in the contact and upper layer; c_g—vertical profile of concentration in the mobile sublayer of the dense layer; u—sediment velocity; u_i—vertical profile of $i-th$ fraction velocity in the contact and upper layer; u_g—vertical profile of velocity in the mobile sublayer of the dense layer; $three-layer\ system$—dense, contact and upper layer; $grain-flow\ sublayer$—mobile sublayer of the dense layer; and $log-profile\ sublayer$—mobile sublayer of the upper layer with the log-profile velocity; h- water depth; $h^* = hcos\xi$.

In relation to this variation in the nature of sediment transport along the depth, for steady flow conditions in an open channel, a three-layer description (Figure 1) was assumed following Kaczmarek et al. [26], which allows not only for determination of the exact distribution of sediment concentration and velocity, but also for mapping the sorting process of heterogeneous sediments. An arrangement of layers was proposed with a continuous description of concentration and velocity profiles in each layer.

The layer at the bottom, according to the assumptions below, has very high concentrations (dense layer) (Figure 1). Transport of highly "packed" grains occurs here, with the closer to the conventional bottom line, the greater the loosening of the water–soil mixture in the dense layer, and the exchange of momentum between grains occurs as a result of their collisions. In relation to the occurrence of high concentrations, it is assumed that all grain fractions move at a given ordinate with equal speed (have equal velocity profiles). This is because interactions between grains are very strong and individual fractions "pull" each other in a water–soil mixture of very high concentration.

The dense layer can be divided into two sublayers. The first, lower sublayer is very strongly "packed" with grains. There are plastic, "Coulomb"-type stresses here. Transport of sediments begins in the higher sublayer of the dense layer, called the grain flow sublayer, where the movement of the water–soil mixture takes place, and the exchange of momentum between grains occurs as a result of their collisions. Due to the very strong interactions between grains, it is proposed to describe the sediment transport in this sublayer with a single representative diameter $d_r = d_{50}$.

Above the dense layer, there is further loosening of the water–soil mixture and exchange of momentum between grains in the process of collisions, with each $i-$th fraction of sediment in this area, characterized by the $i-$th concentration of $c_i(z)$, moves with its own separate $i-$th velocity $u_i(z)$. A process of grain sorting takes place here, with the finer grains remaining in suspension and being lifted higher by turbulence, while the coarser grains fall back to the bottom. This layer is called the contact layer.

The stresses between grains in the contact layer vary from a maximum value τ_0 (at the interface between the dense layer and the contact layer) to the magnitude of τ'_* at the upper boundary of contact layer (Figure 1). It is noteworthy that in the upper sublayer of the dense layer, the stress component τ_0 representing viscous stresses gradually disappears. The vanishing nature of viscosity-type stresses, characteristic in the presented model in the upper part of the dense layer, was confirmed by Cowen et al. [29], who studied shear stress values under laboratory conditions.

The uppermost region is the suspension area (turbulent flow area), which is divided into an inner layer (called log-profile sublayer, where the sediment velocity distribution is assumed to be logarithmic to which the calculated velocity profile inside the contact layer tends) and an outer layer with very low concentrations, where the velocity profile is not necessarily logarithmic.

The boundary conditions between the layers, described by different Equations, are defined in such a way that the distribution of sediment concentrations and velocities is continuous, practically from the zone of complete stillness to the area near the water surface, where the concentrations are already very small. At the upper boundary of the dense layer, the effective stresses τ_0 are equal to:

$$\tau_0 = \gamma^2 \tau'_* \tag{5}$$

where γ is the so-called mobile bottom effect parameter.

In order to determine the parameter γ, it was assumed that the total transport in the dense and contact layers could be compared with the classical empirical formula of Meyer–Peter and Müller [5]. This formula was developed on the basis of a series of sand and gravel fraction transport measurements, was extensively tested, and is the most widely used in engineering practice for calculating the bedload transport, i.e., in this case for transport in the dense and contact layers.

Thus, a relationship can be formulated:

$$q_g + q_c = \Phi_{MPM} \sqrt{(s-1) g d_r^3}, \tag{6}$$

where q_g—sediment transport in the dense layer being a function of friction $\tau_0 = \rho \gamma^2 u'^2_{f*}$; q_c—sediment transport in the contact layer being a function of friction $\tau_0 = \rho u'^2_{f*}$; $s = \rho_s / \rho$—relative density, as a ratio of sediment density to water density, and Φ_{MPM}—dimensionless transport determined by the MPM formula:

$$\Phi_{MPM} = 8\left(\Theta'_* - \Theta_c\right)^{1.5}, \tag{7}$$

where Θ_c—Shields' critical parameter [6], assumed $\Theta_c = 0.05$, and Shields' dimensionless parameter are defined as:

$$\Theta'_* = \frac{\mathrm{u}'^2_{\mathrm{f}*}}{\mathrm{g(s-1)}d_r}. \tag{8}$$

The parameter γ is determined iteratively from Equation (6) [26–28,30].

2.3. Equations in the Dense Layer

Consider the effect of gravitational forces on sediment grains resting on a bed of slope ξ. The gravitational force on the grains can be divided into two components, i.e., parallel to the bottom $(\rho_s - \rho) g sin\xi$, and perpendicular to the bottom $(\rho_s - \rho) g cos\xi$ (Figure 2).

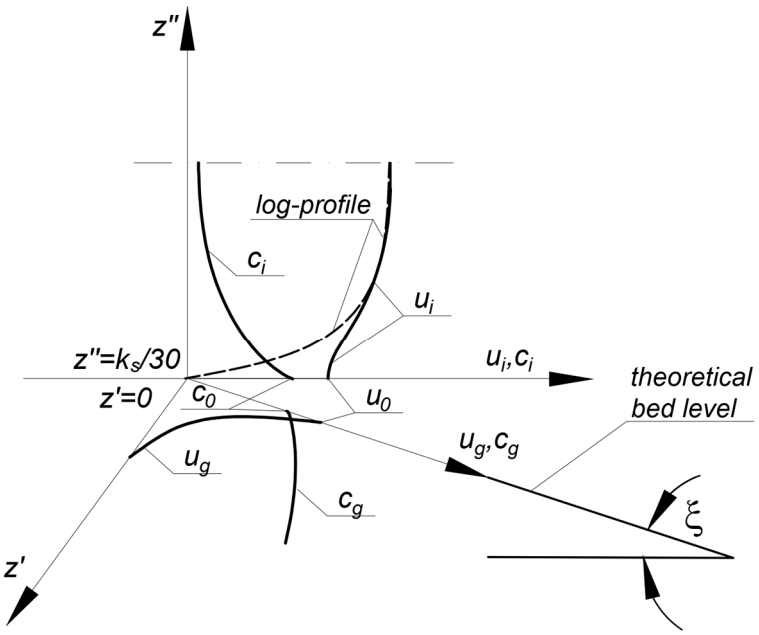

Figure 2. Components of the gravitational force acting on the sediment grain under conditions of sloping bottom at an angle ξ; u_0—velocity at the theoretical bed level (i.e., at the upper boundary of the dense layer).

As the bottom slope increases, the value of the component of gravity parallel to the bottom $(\rho_s - \rho)gsin\xi$ will increase, at the expense of decreasing component perpendicular to the bottom. Thus, the component parallel to the bottom will act together with shear stresses associated with water flow, causing an increase in sediment transport intensity (or the opposite, slowing transport, in the case of locally occurring reverse gradients). Taking the above into account, in the coordinate system with z' axis hooked to the line of theoretical bottom and pointing downward (Figure 2), the balance of vertical and horizontal forces in the dense layer yields the equations in the following form [31]:

$$\alpha^0\left(\frac{c_g - c_0}{c_m - c_g}\right)sin\phi sin2\psi + \mu_1\left(\frac{\partial u_g}{\partial z'}\right)^2 = \tau_0 + (\rho_s - \rho)gsin\xi\int_0^{z'} c_g dz', \tag{9}$$

$$\alpha^0\left(\frac{c_g - c_0}{c_m - c_g}\right)(1 - sin\phi cos2\psi) + \mu_2\left(\frac{\partial u_g}{\partial z'}\right)^2 = \left(\frac{\mu_2}{\mu_1}\right)\Big|_{c_g=c_0}\tau_0 + (\rho_s - \rho)gcos\xi\int_0^{z'} c_g dz', \tag{10}$$

where $\tau_0 = \rho u_{f0}^2$, $\alpha^0 = \rho_s\, g d_r$; c_m—maximum concentration value at the lower boundary of the dense layer; c_0—sediment concentration at the upper boundary of the dense layer, ϕ = quasi-static angle of internal friction, and ψ = angle between the principal axis of stress and the horizontal axis:

$$\psi = \frac{\pi}{4} - \frac{\phi}{2}, \tag{11}$$

μ_2, μ_1—concentration functions (following Sayed and Savage [32]) described as:

$$\mu_1 = \frac{0.03}{(c_m - c_g)^{1.5}}\rho_s d_r^2, \tag{12}$$

$$\mu_2 = \frac{0.02}{(c_m - c_g)^{1.75}}\rho_s d_r^2. \tag{13}$$

where representative diameter d_r in grain flow sublayer is assumed as d_{50}.

Equations (9) and (10) are solved using the iterative method with numerical integration. Solving these equations leads to finding both the sediment velocity $u_g(z')$, as well as the concentration $c_g(z')$ in the dense layer. The concentration $c_g = c_0 = 0.32$, following [26], was adopted as the boundary condition at the upper boundary of the dense layer. First, the course of concentration values is sought until the lower boundary condition is reached, i.e., the maximum concentration, which was adopted as $c_m = 0.53$ [26]. The calculation is carried out only up to the point where $c_g = c_{ms} = 0.5$. This is dictated by the need for the denominators in Equations (12) and (13) not to reach zero when $c_g = c_m = 0.53$. It is assumed that above this concentration value the grains are already maximally "packed" and remain motionless. Here, the boundary condition for velocity $u_g = 0$ is assumed to determine the distribution of velocity $u_g(z')$ throughout the dense layer for the previously calculated concentrations. Thickness of the mobile part of the dense sublayer δ_g is determined for $u_g(z') > 0$. Under intense flow conditions, the mobile sublayer is dominant and covers all or almost all of the dense layer. Conversely, for weak hydrodynamic conditions, almost all of the dense layer is affected by the relation $u_g(z') > 0$, and the thickness of the mobile sublayer practically corresponds to the diameters of individual transported grains.

Under conditions of significant bottom slope, there will be strong soil loosening in the bulk of the dense layer. Thus, in this part, according to [26], it can be assumed $\phi = 24.4^\circ$. However, near the lower boundary of the dense layer, it can be expected that the soil is much less loosened, and the angle of internal friction reaches values close to normative for the type of soil in the compacted state. Following Sobczak [31], it was assumed that the area of linear variation of the angle of internal friction from the magnitude of 24.4° to the normative magnitude in the compacted state is contained in the interval between the region with the loosened sediment in the grain sublayer estimated as the thickness of $10d_r$ (the thickness of mobile sublayer for a non-sloping bottom under very strong hydrodynamic conditions), and the thickness when the concentration in the dense layer c_g reaches the value c_{ms} for the compacted state.

The velocities in the dense layer found in Equations (9) and (10) represent the velocity of the water–grain mixture. Model velocities in the contact layer are the velocities of $i - th$ sediment fraction. The velocity in the log-profile sublayer is identical to the water velocity.

Solving the Equations inside the contact layer (and upward) for each $i-$th fraction leads to finding both the velocity $u_i(z'')$ as well as the concentration $c_i(z'')$. In this case, the axis z'' is directed upward (Figure 2). The method of solution in these layers was discussed in detail in papers [26] for homogeneous sediments and [27] for granulometrically heterogeneous sediments, and more recently in papers [28,30] for non-cohesive granulometrically heterogeneous sediments with cohesive additives. The reader is referred to the mentioned papers for details of the solution.

At this point, it is only worth mentioning that the total sediment transport is calculated as follows:

$$q = \int_{\delta_g}^{0} u_g(z')c_g(z')dz' + \sum_{i=1}^{N} n_i \int_{0}^{\delta_c} u_i(z)c_i(z)dz + \sum_{i=1}^{N} n_i \int_{\delta_c}^{h} u_i(z)c_i(z)dz, \quad (14)$$

where n_i—is the share of particular $i-$th fraction in the grain size distribution, N—is the number of fractions, and δ_c—is the thickness of the contact layer.

3. Discussion of Numerical Calculation Results

Figures 3a,b and 4a,b show the calculated vertical distributions of sediment concentration and velocity in the contact and the dense layers, respectively, at different bottom slopes ranging from -20° to 20° for identical flow and sediment parameters ($\Theta'_* = 0.5$, $d = 0.2$ mm, and $\rho_s = 2650$ kg/m^3). It can be seen that changing the slope angle has a dramatic effect on both the concentration values inside the contact layer (Figure 3a) and upward, as well as on sediment velocities in this area (Figure 3b) and on velocities and concentrations inside the dense layer (Figure 4a,b). Negative gradients correspond

to gradients opposite the flow direction. Of course, this is possible only in local, short sections of the bottom, where there are large bottom formations or underwater thresholds at which material accumulation occurred. In such cases, the component of gravitational forces acting on the sediment grains parallel to the bottom will act opposite to the shear stresses associated with the flow. The results presented here show that in such a case, the concentrations, velocities, and thicknesses of the active (mobile) sublayer inside the dense layer are significantly smaller compared to situations with a positive gradient.

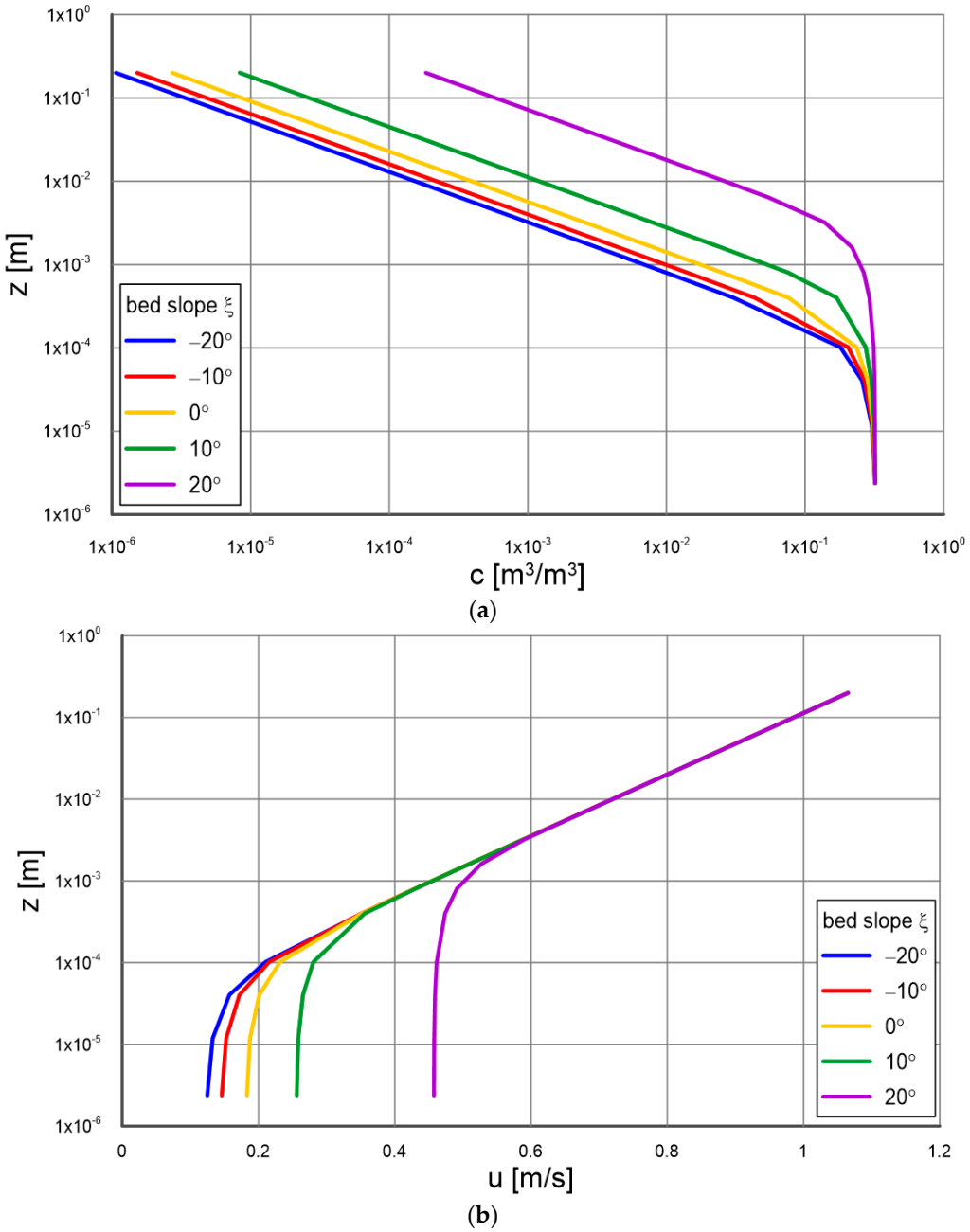

Figure 3. (**a**) Calculated vertical distributions of sediment concentration in the contact layer at different bottom slopes for equal flow and sediment parameters ($\Theta'_* = 0.5$, $d = 0.2$ mm, and $\rho_s = 2650$ kg/m^3). (**b**) Calculated vertical distributions of sediment velocity in the contact layer at different bottom slopes for equal flow and sediment parameters ($\Theta'_* = 0.5$, $d = 0.2$ mm, and $\rho_s = 2650$ kg/m^3).

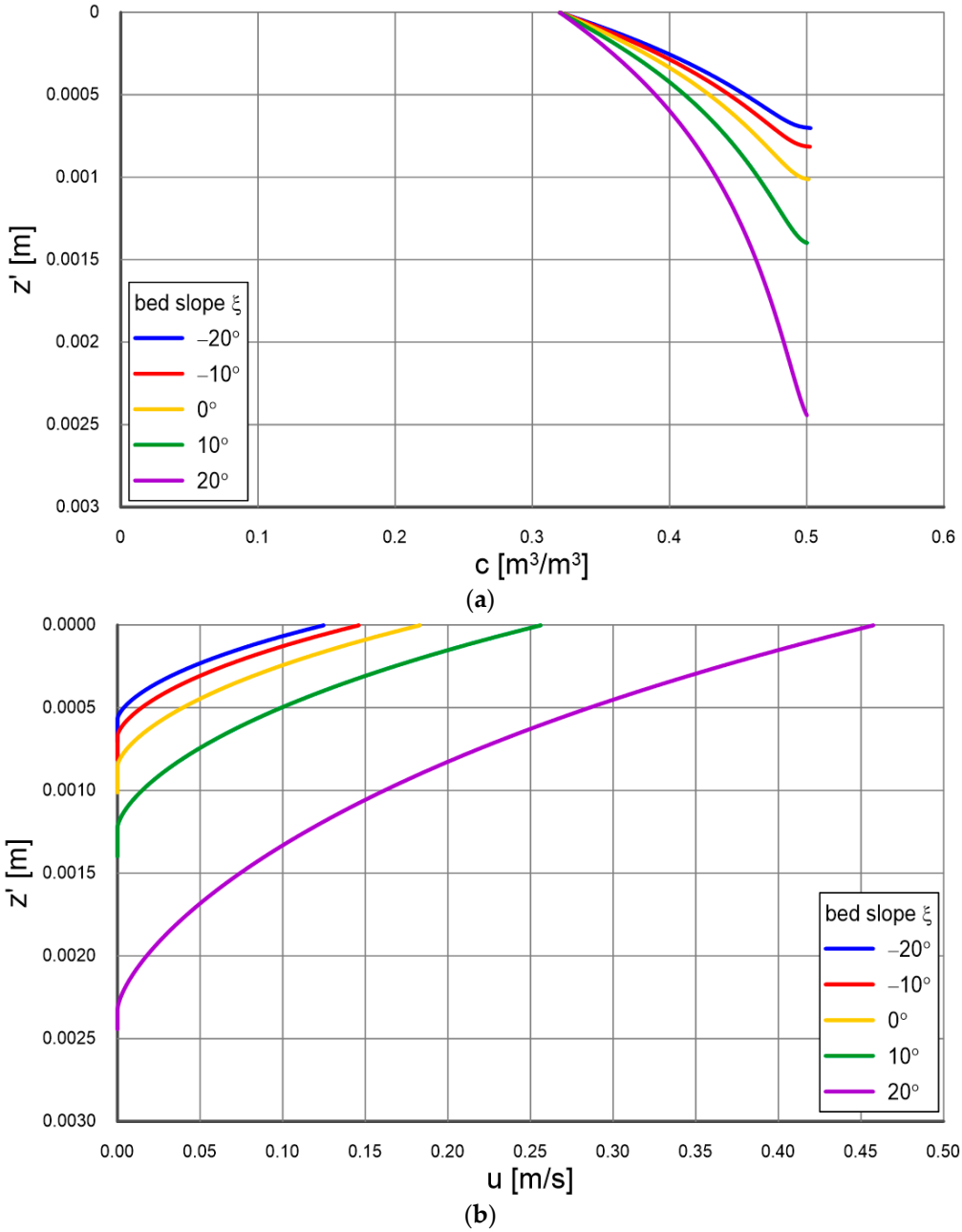

Figure 4. (**a**) Calculated vertical distributions of sediment concentration in the dense layer at different bottom slopes for equal flow and sediment parameters ($\Theta'_* = 0.5$, $d = 0.2$ mm, and $\rho_s = 2650$ kg/m^3). (**b**) Calculated vertical distributions of sediment velocity in the dense layer at different bottom slopes for equal flow and sediment parameters ($\Theta'_* = 0.5$, $d = 0.2$ mm, and $\rho_s = 2650$ kg/m^3).

Figure 5 shows the calculated transport intensities in the dense layer and the contact layer and upward at different bottom slopes for the present case ($\Theta'_* = 0.5$, $d = 0.2$ mm, and $\rho_s = 2650$ kg/m^3). It is interesting that as the bottom slope increases, the increase in transport values in the contact layer is more intense than in the dense layer. This is because the model satisfactorily reproduces the greater "loosening" of sediments in the bottom in the case of significant slopes. Therefore, the presented example results of transport calculations are intuitive and reasonable, as the result of such "loosening" of greater transport will occur in the contact layer, due to the dramatic increase in velocity at its lower boundary, where transport is dominated by momentum exchange via grain collisions. As a result, there will also be significantly higher concentrations of suspended sediment further from the bottom (Figure 5).

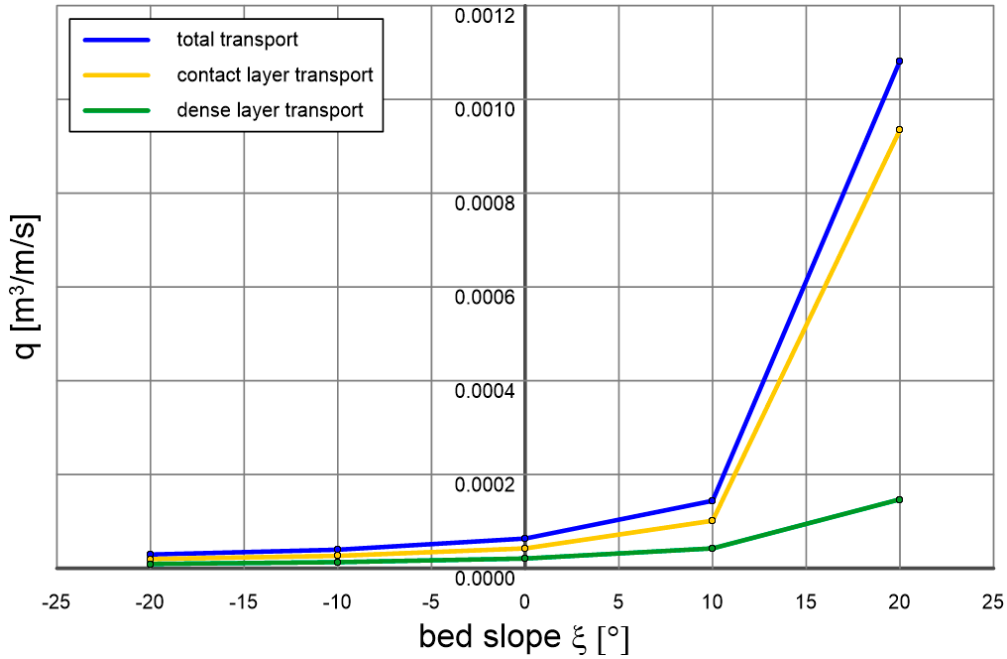

Figure 5. Calculated sediment transport in the dense and contact layers for different bottom slopes with equal flow and sediment parameters ($\Theta'_* = 0.5$, $d = 0.2$ mm, and $\rho_s = 2650$ kg/m^3).

4. Discussion of Calculation Results in Comparison with Measurements

4.1. Vertical Profiles of Velocity, Concentration and Grain Size Distribution

Frey [33] conducted measurements under laboratory conditions for homogeneous surrogate sediment consisting of glass beads with a diameter of $d = 6$ mm at a constant gradient of 10%, under flow intensities corresponding to dimensionless friction in the range $\Theta'_* = 0.076 \div 0.1$. He carried out the observations using a special camera that allows for recording images at 130 frames per second. However, in order to record individual grains selectively, the width between the vertical panes of flow channel walls was chosen to ensure that there was only one "vertical" layer of beads.

In order to compare the measurement results with calculations for specific conditions, calculations were carried out with the three-layer model presented in this paper.

Figure 5 in paper [33] shows the original vertical distributions of both velocity and concentration presented by Frey for four measurement series, designated by the author as N10-x, where 10 stands for the bottom slope in percentage and "x" is the designation of the specific measurement series under given conditions. Calculation results with the multilayer model for selected series of Frey [33] measurements are shown in Figure 6. The calculated concentration and velocity distributions for two measurement series are shown: N10-6 for $\Theta'_* = 0.076$ and N10-16 for $\Theta'_* = 0.1$, with fixed diameter $d = 6$ mm and bottom slope of 10%. The data presented are calculation results in three layers of the model, i.e., in the dense layer (z'/d axis pointing downward) and in the contact layer and upward (z''/d axis pointing upward).

It should be noted that the maximum concentration boundary values adopted for the calculations differ slightly from the measured values, at the lower boundary of the dense layer $(0.5 - 0.56)$. However, this does not fundamentally affect the transport due to the zero sediment velocities occurring in this area. Comparing the calculation results (Figure 6) with the corresponding distributions determined by Frey, shown in Figure 5 in the paper [33], it can be seen that the nature of velocity and concentration distributions are very similar. This confirms the validity of theoretical assumptions made for the lowest layers of the model, from the motionless zone, through the layer to the suspension zone.

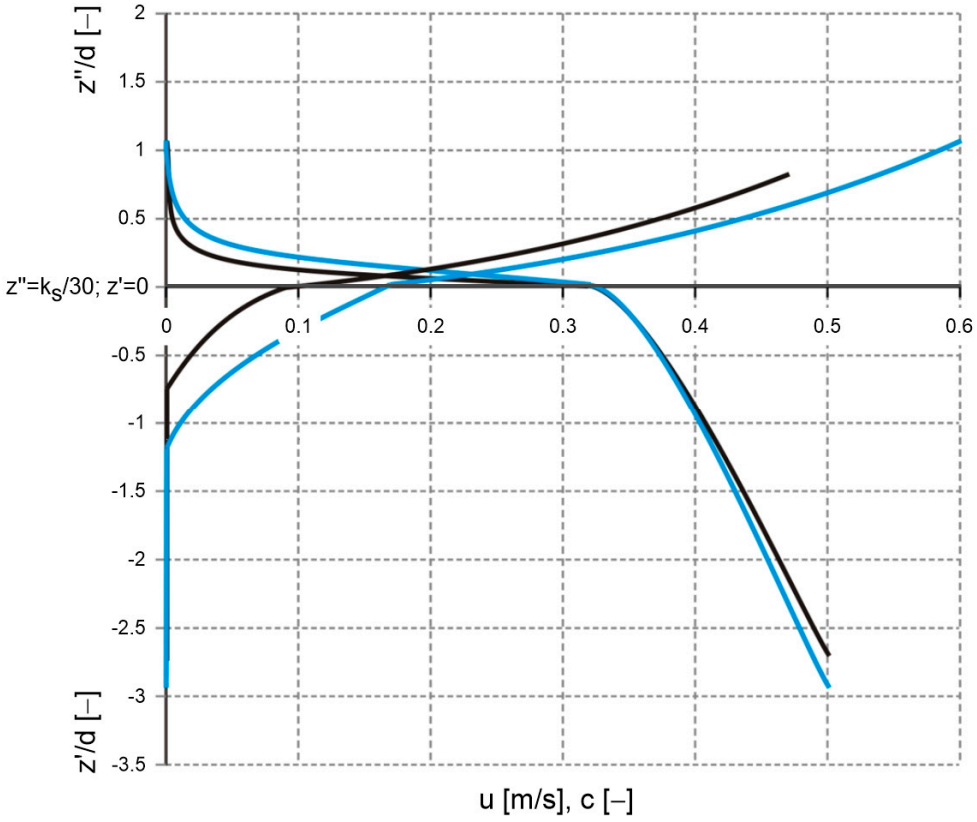

Figure 6. Calculated velocities and sediment concentrations with the multilayer model for parameters corresponding to test measurements by Frey [33] N10-6 (black lines) and N10-16 (blue lines).

There are, of course, some differences, with the model's overestimation of sediment velocity in the upper zone shown in Figure 6 compared to Figure 5 in [33] being particularly noticeable. However, it is difficult to clearly address the model's errors, as the tests took place on surrogate sediment of balls of equal diameter transported in a single vertical layer. Under such conditions, the real dynamics of grains (here, glass balls) are greatly influenced by the channel walls in the immediate vicinity.

Calculated sediment velocities and concentrations in the dense layer compared to measurements by Frey (Figure 5 in [33]) are mapped much better than in the contact layer. This may be related to the fact that this area is dominated by strong interactions between grains. Therefore, the above-mentioned effect of wall influence is most likely no longer as important as it is during fusion and faster grain movement. In the contact layer and upward, the calculated grain velocities are overestimated, because under natural conditions grains collide with other grains with similar velocities, while in the laboratory, based on measurements described by Frey [33], grains transported in one vertical layer "bump" against the channel walls, which are at rest. Therefore, friction is of great importance here under laboratory conditions and has the effect of slowing down the beads.

The calculated concentration values in the contact layer seem to decrease much more intensively with the distance from the boundary of two layers. However, it should be noted that the transport intensities calculated with the presented model in comparison with the transports calculated on the basis of Frey's measurements [33] (Figure 7) provide satisfactory results.

In summary, when taking into account the measurement conditions, as well as the fact of replacing real sediment with glass beads, it can be stated that the consistency of measurement results with calculations is satisfactory.

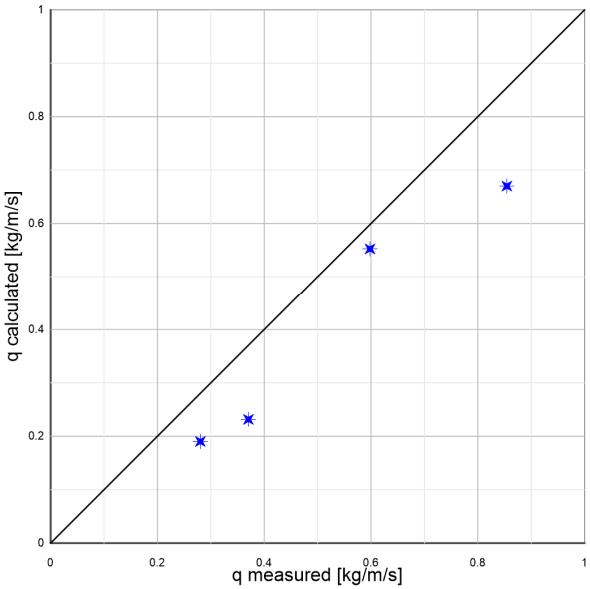

Figure 7. Example transports of sediments represented by 6 mm diameter glass beads measured by Frey [33] under 10% bottom slope conditions against the results of calculations (following [31]) with the presented multilayer model. The points from lowest to highest represent successive tests for dimensionless friction values, respectively: $\Theta'_* = 0.076, \Theta'_* = 0.08,\ \Theta'_* = 0.1,$ and $\Theta'_* = 0.106$.

One of the more interesting papers describing the vertical distribution of sediment concentration and segregation is the study by Damgaard et al. [34], who conducted measurements of fine sand transport by determining concentration and velocity profiles in a channel that allows the implementation of a bottom slope. They made measurements using granulometrically heterogeneous sediments with a median $d_{50} = 0.23$ mm under conditions of dimensionless friction $\Theta'_* = 0.06 \div 0.5$, varying the bottom slope from $\pm 10^\circ$ to $\pm 20^\circ$.

Figures 8 and 9 show a comparison of calculation results with measurements of velocity and concentration distributions for conditions defined by the dimensionless friction $\Theta'_* = 0.06$. The first figure shows results for gradients consistent with the direction of flow, and the second figure shows results for opposite gradients (marked with "-"). It can be seen that the model reflects sediment velocities very well and reproduces concentration distributions well. The highest concentration correspondences are found for significant gradients ($\pm 20^\circ$), while for smaller gradients ($\pm 10^\circ$), relatively large differences are observed, which are most likely due to the presence of bottom forms (ripples), which are particularly strong at smaller gradients.

Damgaard et al. [34] also devoted attention to the vertical segregation structure of heterogeneous sediments under conditions of different bottom slopes. The authors measured the concentration of individual sediment fractions at different distances from the bottom and presented the results in the form of vertical variation of the characteristic diameter d_{50}. The parameters corresponding to each test (values of dynamic velocity, dimensionless friction and bottom slope) are shown in Table 1. Calculation results against the measurement results for the selected series are shown in Figures 10 and 11, while the vertical variation of the median d_{50} of suspended sediments at height z was calculated from the obtained concentration distributions according to the Equations:

$$c(z) = \sum_{i=1}^{N} n_i c_i(z)\ , \tag{15}$$

$$m_i(z) = \frac{c_i(z)}{c(z)}. \tag{16}$$

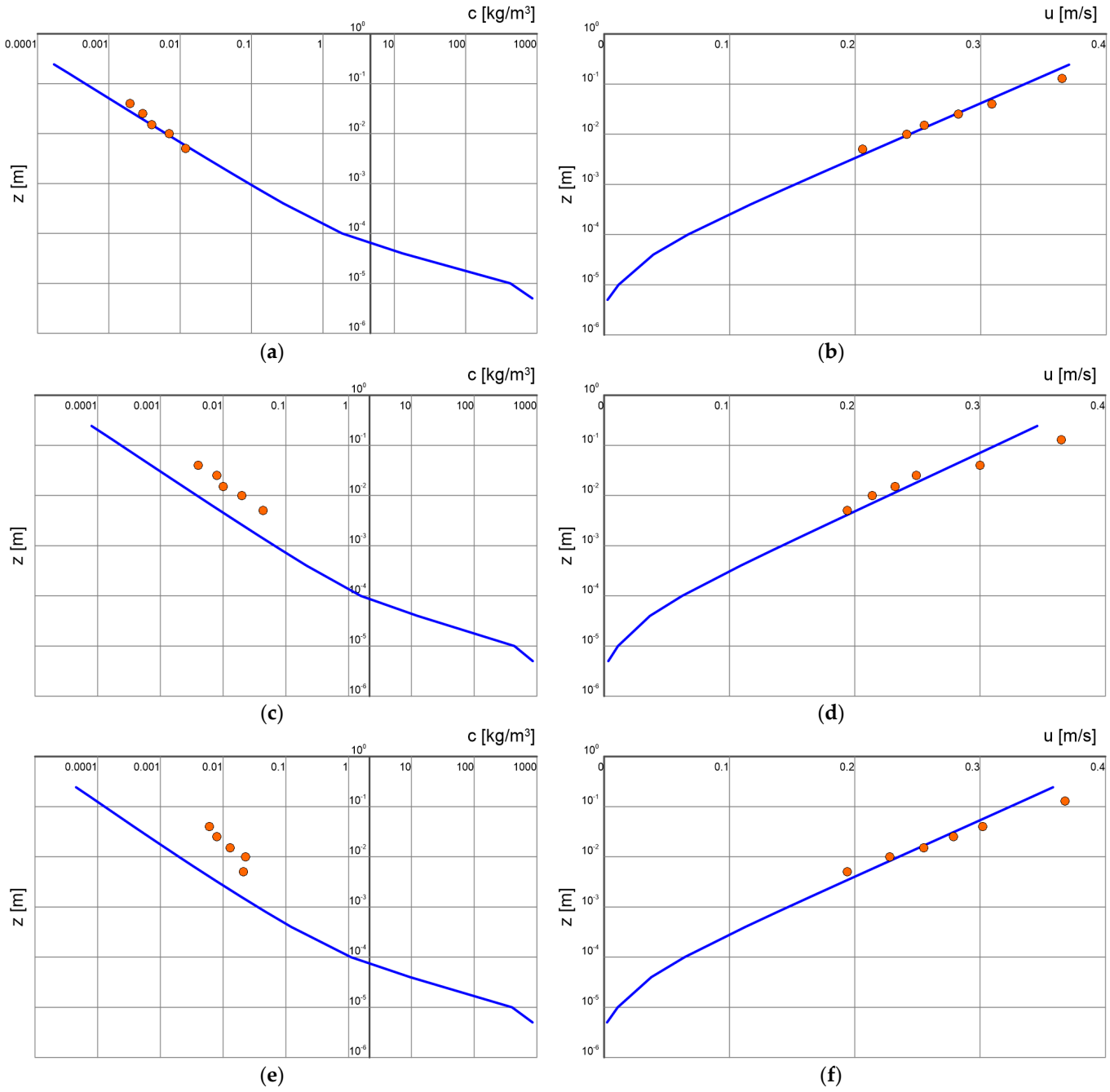

Figure 8. Comparison of distributions of velocity and sediment concentration in the contact and upper layers for different bottom slopes ξ ($d_{50} = 0.23$ mm, $\Theta'_* = 0.06$): (**a**,**b**) $\xi = 20^\circ$; (**c**,**d**) $\xi = 10^\circ$; and (**e**,**f**) $\xi = 0^\circ$ calculated with three-layer model (lines) and measured (points) by Damgaard et al. [34].

Knowing the calculated fractional content m_i at a given level z, it is easy on this basis to estimate the median $d_{50}(z)$.

The lines represent the calculation results, and the points represent the values of d_{50} from measurements, i.e., obtained from the measured concentrations of individual fractions. The lowest value d_{50} of the lines representing calculation results (0.23 mm) corresponds to the characteristic diameter of the sediment at the bottom. As can be seen in the figures, the quality of prediction of the vertical structure d_{50} in the area above the intensive sorting zone is a test of the validity of theoretical assumptions and the adopted sorting model in the layers below.

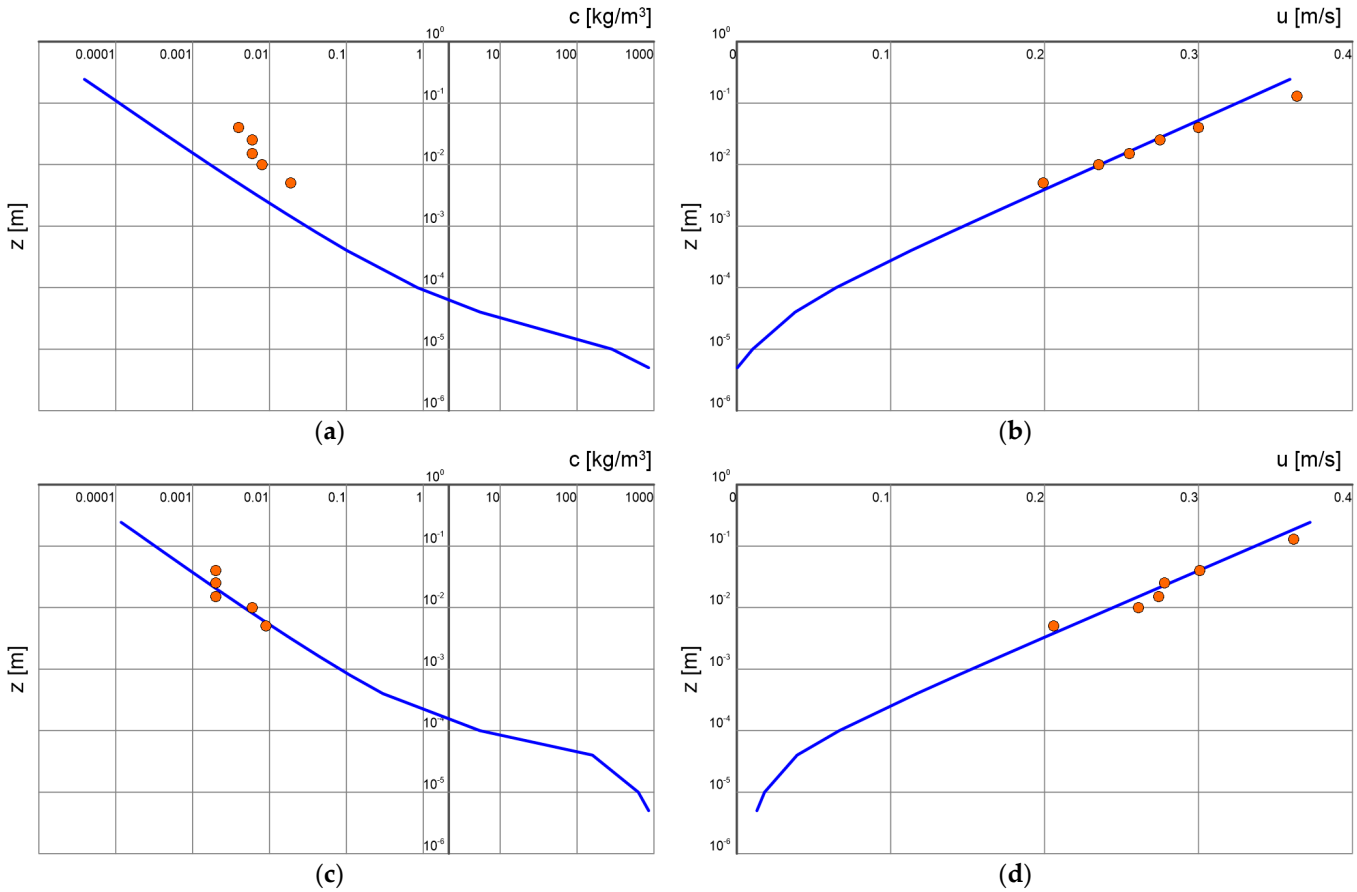

Figure 9. Comparison of distributions of velocity and sediment concentration in the contact and upper layers for bottom slopes ξ opposite the flow direction ($d_{50} = 0.23\ mm$, $\Theta'_* = 0.06$): (**a**,**b**) $\xi = -10°$; and (**c**,**d**) $\xi = -20°$ calculated with multilayer model (lines) and measured (points) by Damgaard et al. [34].

Table 1. Values of bottom slopes and dimensionless friction for selected measurement series by Damgaard et al. [34] used to verify the model for the prediction of vertical sorting of granulometrically heterogeneous sediment.

$\xi = 20°$	Test 1 $u_{f*} = 0.0157$ $\theta'_* = 0.064$	Test 2 $u_{f*} = 0.0217$ $\theta'_* = 0.121$	Test 3 $u_{f*} = 0.0299$ $\theta'_* = 0.230$
$\xi = 10°$	Test 4 $u_{f*} = 0.0147$ $\theta'_* = 0.055$	Test 5 $u_{f*} = 0.023$ $\theta'_* = 0.136$	Test 6 $u_{f*} = 0.0301$ $\theta'_* = 0.233$
$\xi = 0°$	Test 7 $u_{f*} = 0.0154$ $\theta'_* = 0.061$	Test 8 $u_{f*} = 0.0215$ $\theta'_* = 0.119$	Test 9 $u_{f*} = 0.0298$ $\theta'_* = 0.229$
$\xi = -10°$	Test 10 $u_{f*} = 0.0154$ $\theta'_* = 0.061$	Test 11 $u_{f*} = 0.0207$ $\theta'_* = 0.111$	Test 12 $u_{f*} = 0.0287$ $\theta'_* = 0.213$
$\xi = -20°$	Test 13 $u_{f*} = 0.0160$ $\theta'_* = 0.066$	Test 14 $u_{f*} = 0.0198$ $\theta'_* = 0.101$	Test 15 $u_{f*} = 0.0277$ $\theta'_* = 0.198$

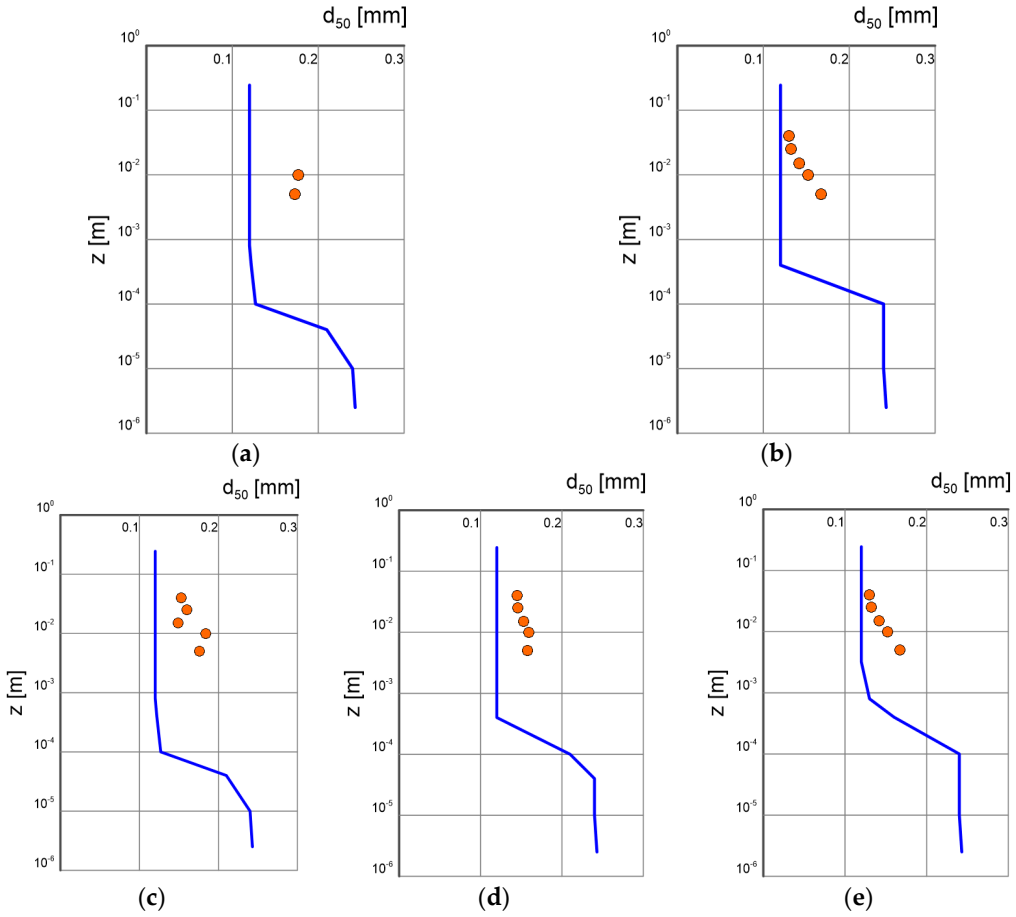

Figure 10. Calculated vertical distributions of the variation in characteristic diameter d_{50} (lines) against the measurement results by Damaard et al. [34] (points) for conditions of bottom slope $\xi = 20^\circ$ (tests 1, 2, (**a**,**b**)) and $\xi = 10^\circ$ (tests 4, 5, and 6, (**c**–**e**)) for different conditions of dimensionless friction (see Table 1). The measured diameter of sediment at the bottom $d_{50} = 0.23$ mm.

4.2. Sediment Transport

Luque [35] conducted a series of measurements of sediment transport in a channel 8 m long, 20 cm high, and 10 cm wide with a design that allowed for a bottom slope. Flow in the channel was generated using a pump. Measurements were conducted for flow with no slope (0°) and three different bottom slopes: 12°, 18°, and 22° under conditions of dimensionless friction in the range $\Theta'_* = 0.03 \div 0.08$. The author studied transport of heterogeneous sediments, which he described by characteristic diameters d_{50}. Measurements for the verification of presented model are very interesting, as Luque [35] used a wide range of materials representing sediments both in terms of not only diameters, but also density:

- sand with density $\rho_s = 2640 \mathrm{kg/m^3}$ and diameters $d_{50} = 0.9$mm and 1.8mm;
- gravel with density $\rho_s = 2640 \mathrm{kg/m^3}$ and diameter $d_{50} = 3.3$mm;
- particles of shelled walnut with density $\rho_s = 1340\ \mathrm{kg/m^3}$ and diameter $d_{50} = 1.5$ mm;
- magnetite grains with density $\rho_s = 4580\ \mathrm{kg/m^3}$ and diameter $d_{50} = 1.8$ mm.

To calculate shear stresses, the authors measured water velocity distributions. Sediment transport was determined using an optical method, based on analysis of recorded films made for grains traveling a certain distance in a given time.

For the direct values of shear stress and sediment and bottom slope characteristics presented by Luque [35], calculations were conducted with the model presented in this paper. Comparisons of calculated and measured transport intensities expressed in terms of dimensionless transport Φ are shown in Figures 12–16. The solid lines indicate a 1:1 correspondence of the calculation results with the measured data, while the dashed lines

indicate the limits of double determination error. The dimensionless transport Φ according to Equation (6) is defined as follows:

$$\Phi = \frac{q}{\sqrt{(s-1)gd^3}}. \tag{17}$$

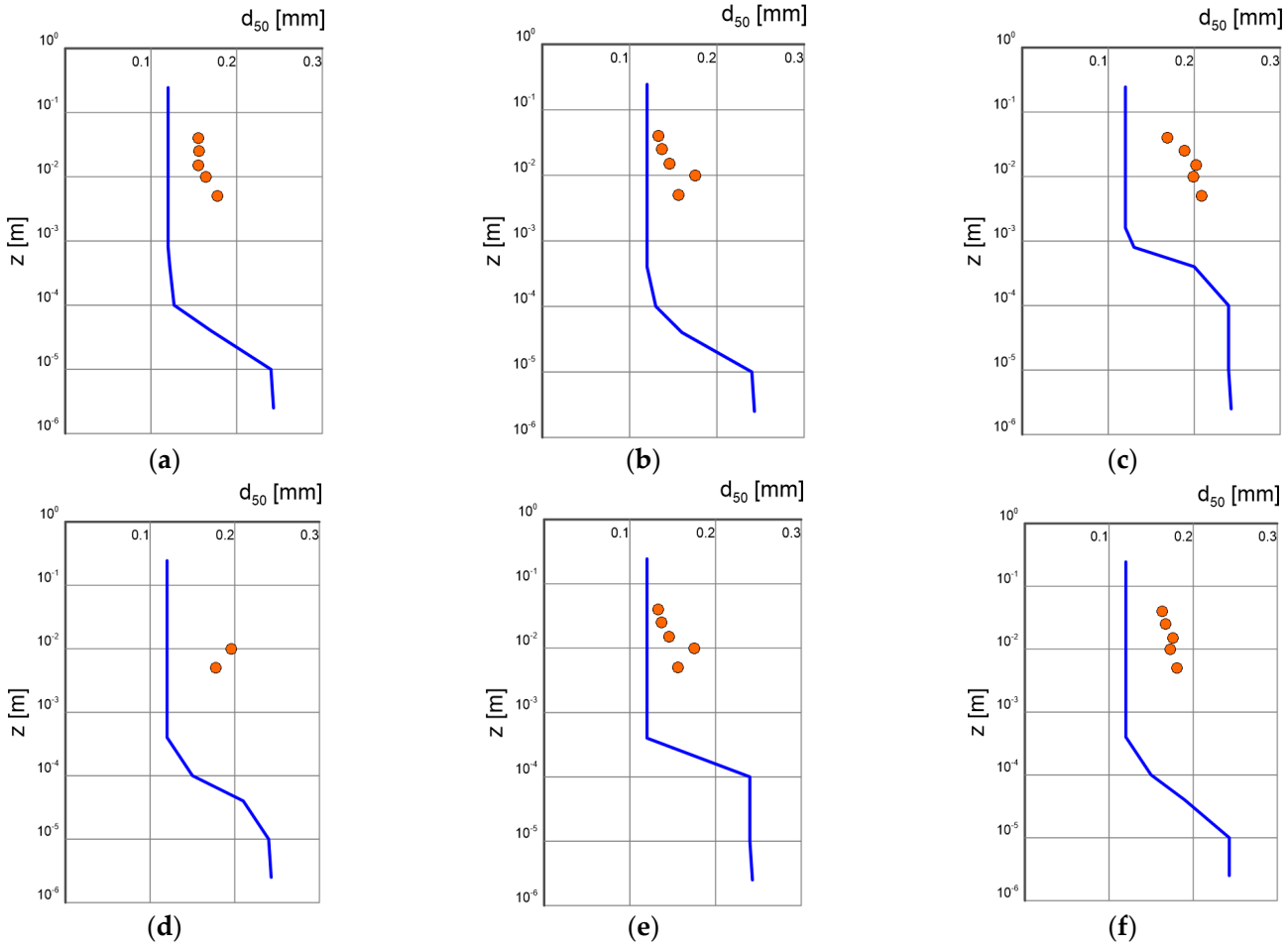

Figure 11. Calculated vertical distributions of the variation in characteristic diameter d_{50} (lines) against the measurement results of Damaard et al. [34] (points) for conditions of bottom slope $\xi = -10°$ (tests 10, 11, and 12, (**a**–**c**)) and $\xi = -20°$ (tests 13, 14, and 15, (**d**–**f**)) for different conditions of dimensionless friction (see Table 1). The measured diameter of sediment at the bottom $d_{50} = 0.23$ mm.

Analyzing the results shown in the above graphs, it can be concluded that the model reproduces sediment transports quite well, regardless of diameter and density, over the full range of bottom slopes used in the experimental studies. Most of the prediction results do not exceed double determination errors. It is worth mentioning that the results of Lugue measurements [35] are characterized by significant deviations from the average values of measurement series. Under conditions close to the beginning of sediment movement, such deviations are typical. Therefore, it is not possible to speak unequivocally about the error of calculation results here. It is interesting to note that there is no decisive difference in the quality of prediction of typical (sandy) sediments from substitute sediments with atypical densities (several times lower or higher). This is a good indication of the model, which may consequently have important implications for future engineering applications.

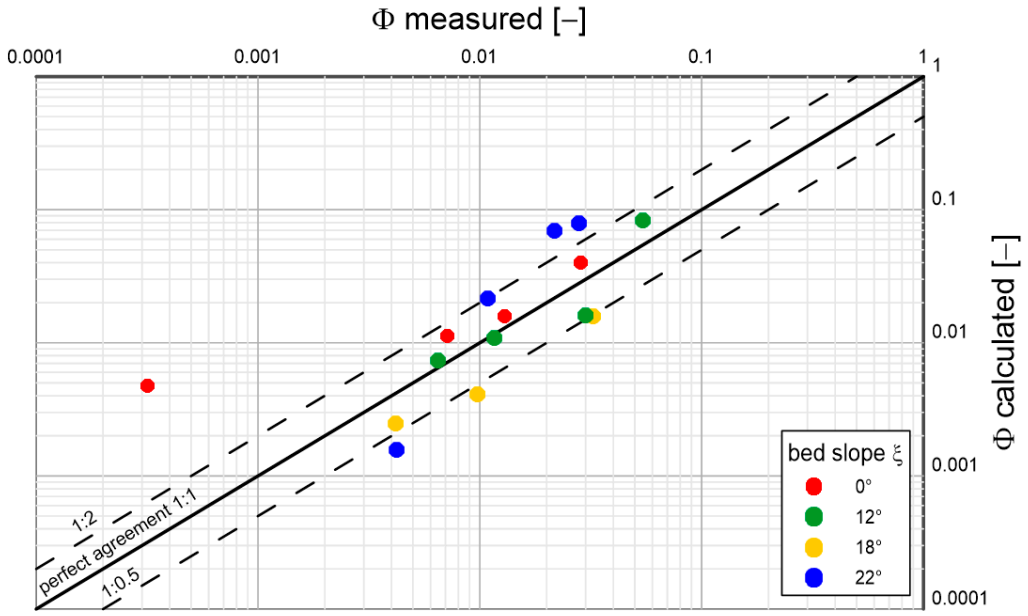

Figure 12. Comparison of calculated and measured transport intensities for sandy sediment with a diameter $d_{50} = 0.9$ mm and density $\rho_s = 2640$ kg/m^3 under conditions of different bottom slopes; $\Theta'_* = 0.03 \div 0.08$ (based on Luque's laboratory studies [35]).

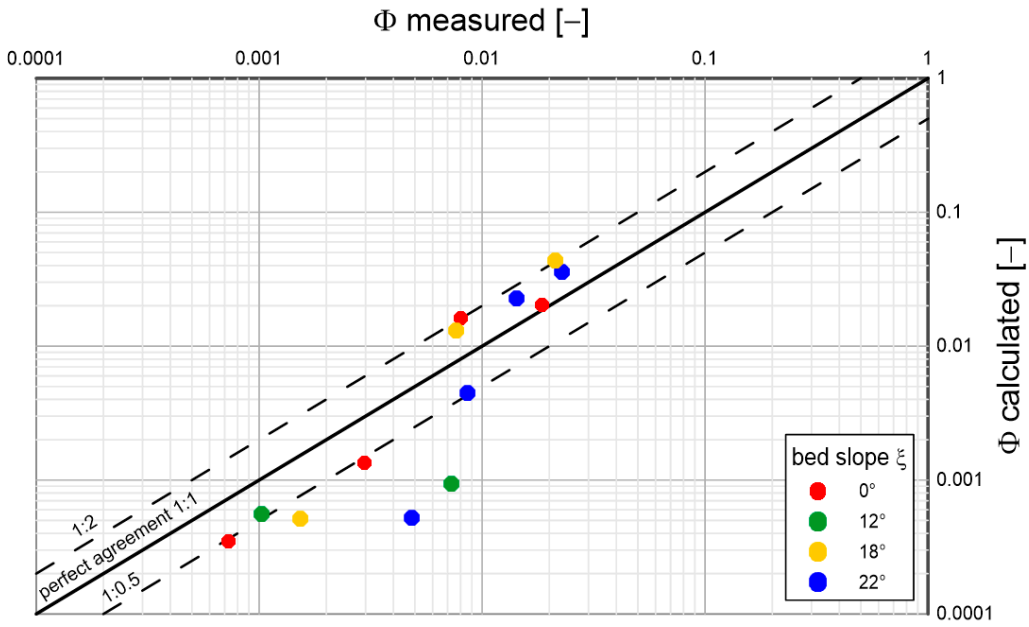

Figure 13. Comparison of calculated and measured transport intensities for sandy sediment with a diameter $d_{50} = 1.8$ mm and density $\rho_s = 2640$ kg/m^3 under conditions of different bottom slopes; $\Theta'_* = 0.03 \div 0.08$ (based on Luque's laboratory studies [35]).

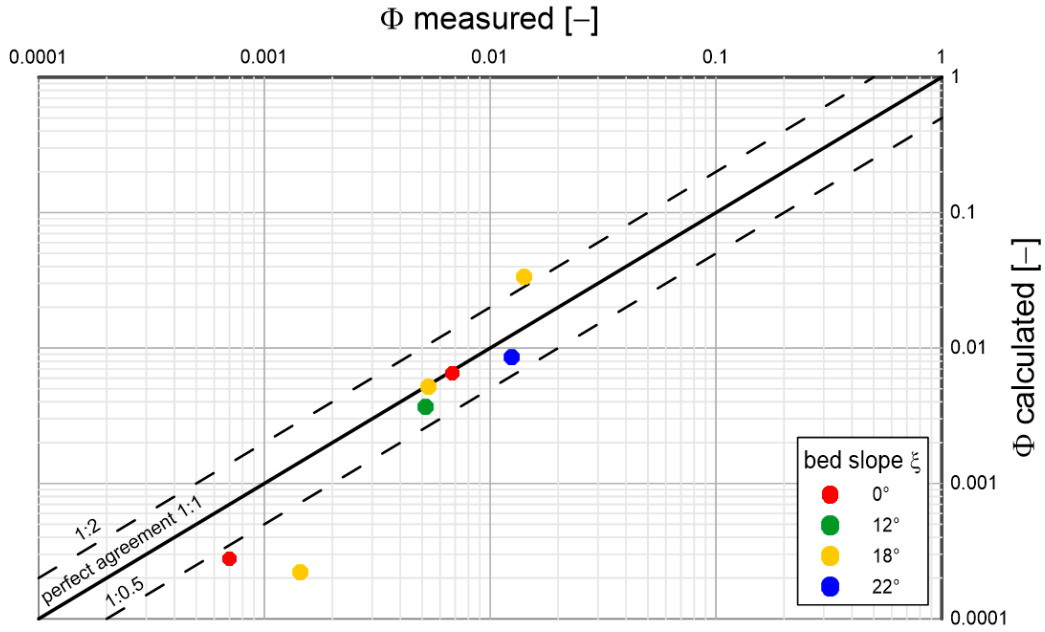

Figure 14. Comparison of calculated and measured transport intensities for sandy sediment with a diameter $d_{50} = 3.3$ mm and density $\rho_s = 2640$ kg/m^3 under conditions of different bottom slopes; $\Theta'_* = 0.03 \div 0.08$ (based on Luque's laboratory studies [35]).

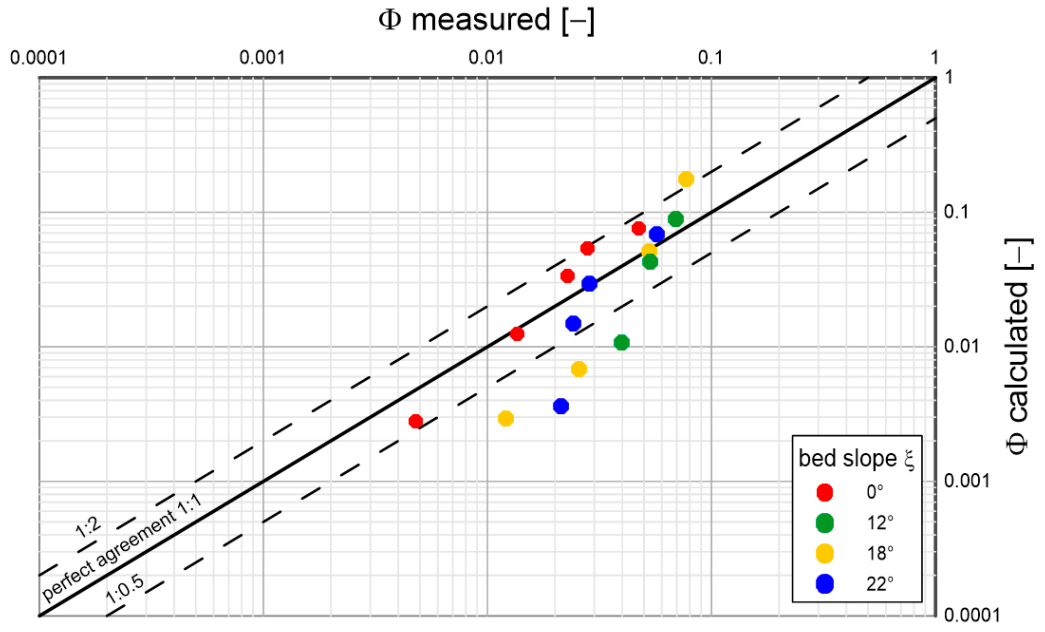

Figure 15. Comparison of calculated and measured transport intensities for sandy sediment with a diameter $d_{50} = 1.5$ mm and density $\rho_s = 1340$ kg/m^3 under conditions of different bottom slopes; $\Theta'_* = 0.03 \div 0.08$ (based on Luque's laboratory studies [35]).

Figure 17 shows a comparison of calculated sediment transport values with selected measured data from Damgaard et al. [34] for heterogeneous sediment with the diameter $d_{50} = 0.237$ mm under conditions of dimensionless friction $\Theta'_* = 0.06 \div 0.2$ with gradients ranging from -20° to 20°. From Figure 17, it can be seen that the data in the graph are arranged in three groups, corresponding to three different flow conditions according to the dimensionless friction values described in the graph Θ'_*. A very good consistency between calculation results and measurements was obtained.

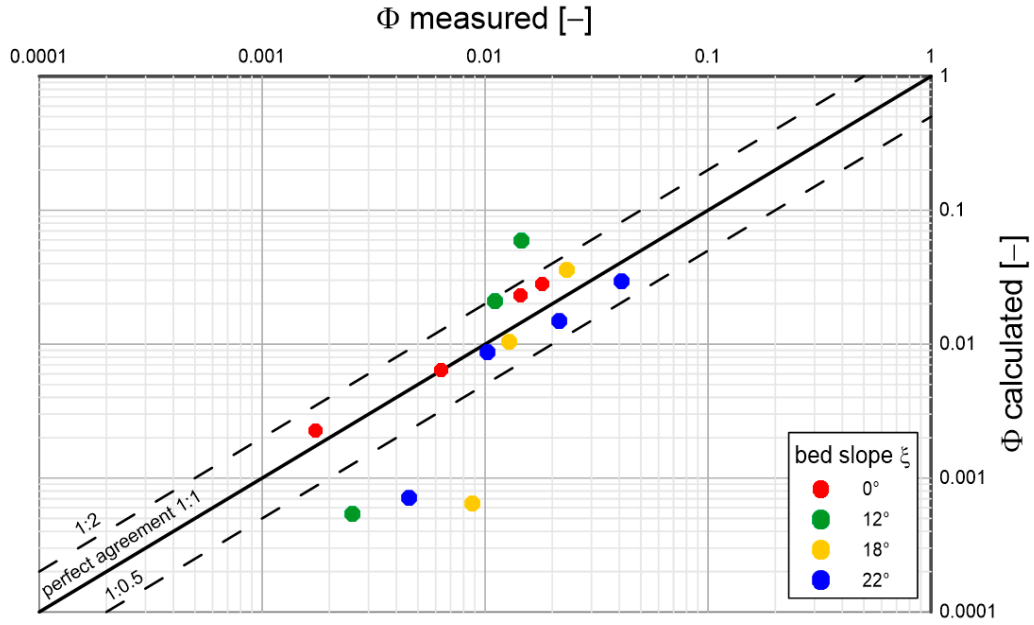

Figure 16. Comparison of calculated and measured transport intensities for sandy sediment with a diameter $d_{50} = 1.8$ mm and density $\rho_s = 4580$ kg/m^3 under conditions of different bottom slopes; $\Theta'_* = 0.03 \div 0.08$ (based on Luque's laboratory studies [35]).

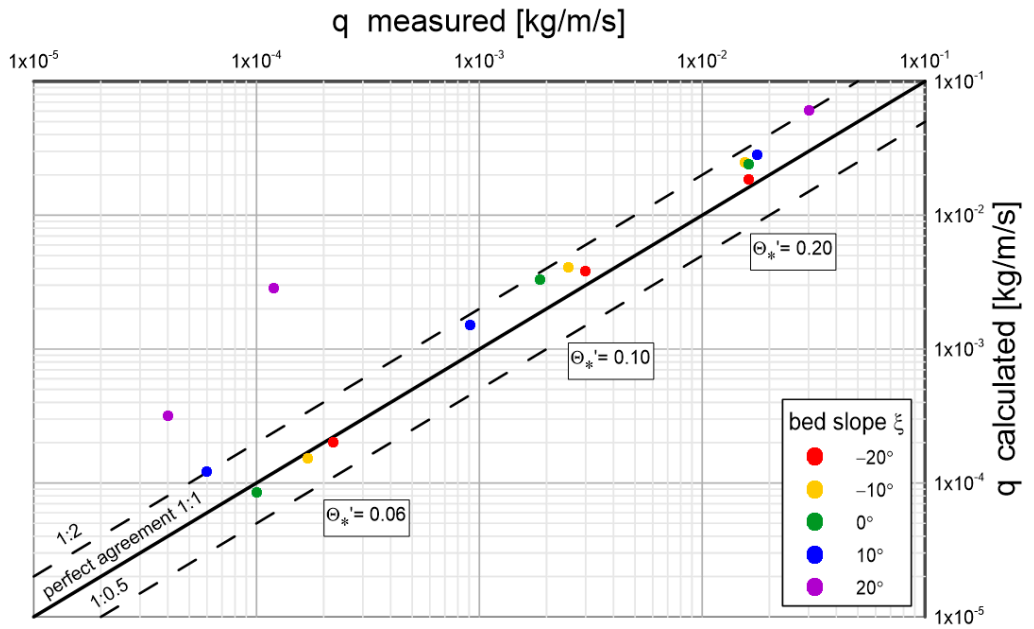

Figure 17. Results of sediment transport calculations compared with measured data by Damgaard et al. [34] for sediment with diameter of $d = 0.237$ mm under conditions of dimensionless friction $\Theta'_* = 0.06 \div 0.2$ with gradients ranging from $-20°$ to $20°$.

Further results of laboratory measurements that were used to verify the presented model under conditions of higher gradients were published by Smart and Jaeggi [36]. The authors conducted measurements of dragged sediment transport using a design that allowed the bottom to slope up to 40°.

Smart and Jaeggi [36] conducted transport measurements of four types of gravels with the following parameters: $d_{50} = 4.3$ mm and density $\rho_s = 2670$ kg/m^3, $d_{50} = 4.2$ mm and density $\rho_s = 2670$ kg/m^3, $d_{50} = 2.0$ mm and density $\rho_s = 2680$ kg/m^3, and $d_{50} = 10.5$ mm and density $\rho_s = 2680$ kg/m^3, with bottom slopes of 3, 5, 7, 10, 15, and 20% for different values of dimensionless friction in the range $\Theta'_* = 0.2 \div 2.35$.

A comparison of calculation results with measurements is shown in Figure 18. Satisfactory conformity was obtained, and in the case of the finest sediments ($d_{50} = 2.0$ mm), very good conformity. It should be noted that the most deviating results ($d_{50} = 10.5$ mm, the lowest extreme point on the graph) were achieved for conditions at the boundary of the beginning of the movement, where concentrations are very small, and the measurements are usually characterized by significant scatterings of the results (single grains starting movement).

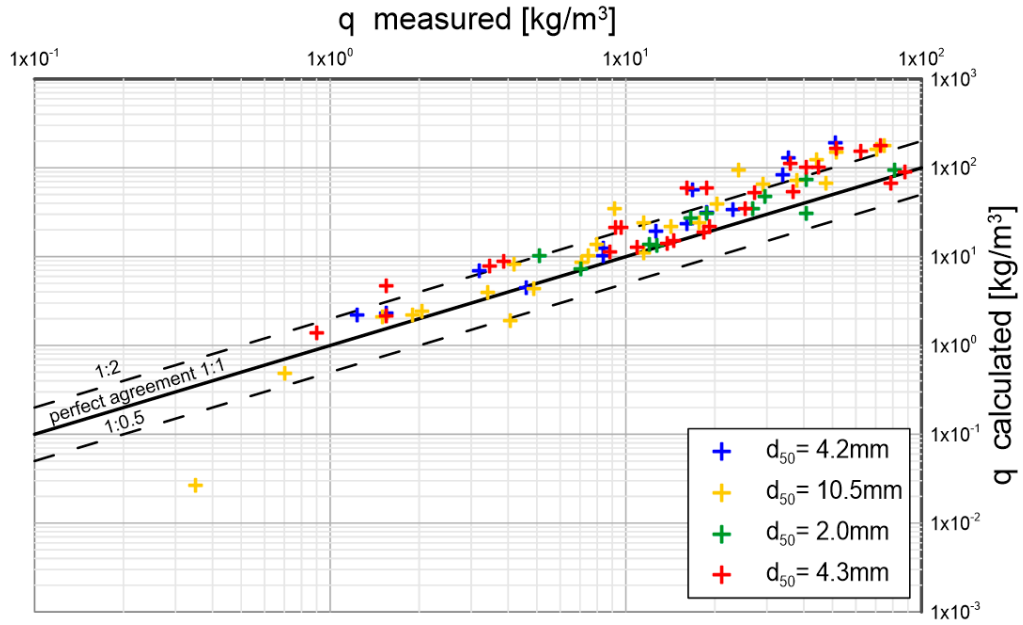

Figure 18. Comparison of sediment transport values calculated by the three-layer model with the results of Smart and Jaeggi's measurements [36] for four different diameters and different values of dimensionless friction in the range $\Theta'_* = 0.2 \div 2.35$ in the range of bottom slopes from 3 to 20%.

Larionov et al. [37] published the measurement results of sediment transport, which they conducted in a channel that allowed the realization of slopes up to 35%. In the experiments they used four different heterogeneous sediments with characteristic diameters $d_{50} = 0.75,\ 0.108,\ 1.25,$ and 1.75 mm. Tests were carried out for the full range of dimensionless friction in the range from values close to the onset of grain motion ($\Theta'_* = 0.06$), with small bottom slopes close to 0.5%, to strongly developed, intensive transport (max. value $\Theta'_* = 4$ with bottom slopes up to 35%). Figure 19 shows a comparison of the measured results with the values calculated with the three-layer model. The consistency is satisfactory. In most cases, the results are within double determination error.

Aziz and Scott's [38] measurement results are also used to verify the presented three-layer model under bottom slope conditions. Figure 20 shows a comparison of calculated sediment transport intensities for selected measurement results carried out by the authors for sediment with a diameter of $d = 0.5$ mm, with bottom slopes of 3% and 10%, corresponding to two groups of dimensionless friction values in the range $\Theta'_* = 0.16 \div 0.29$ and $\Theta'_* = 0.44 \div 0.76$. Again, very good conformity of calculation results with measured values was obtained.

Recking et al. [11] conducted measurements of a homogeneous sediment transport granulometric in a circulation channel for bottom slopes of 0–10% in the range of conditions from the beginning of movement ($\Theta'_* = 0.06$) to developed transport ($\Theta'_* = 0.29$). Calculation results against measured data for selected three diameters ($d = 2.3,\ 4.9,$ and9 mm) are shown in Figure 21. The model reproduces the measured transport values very well. The exceptions are the lowest points, concerning measurements under conditions close to the beginning of debris movement (Θ'_* close to the value of 0.06), when practically single

grains are mobile. However, under such conditions, there are also significant discrepancies in the measurements.

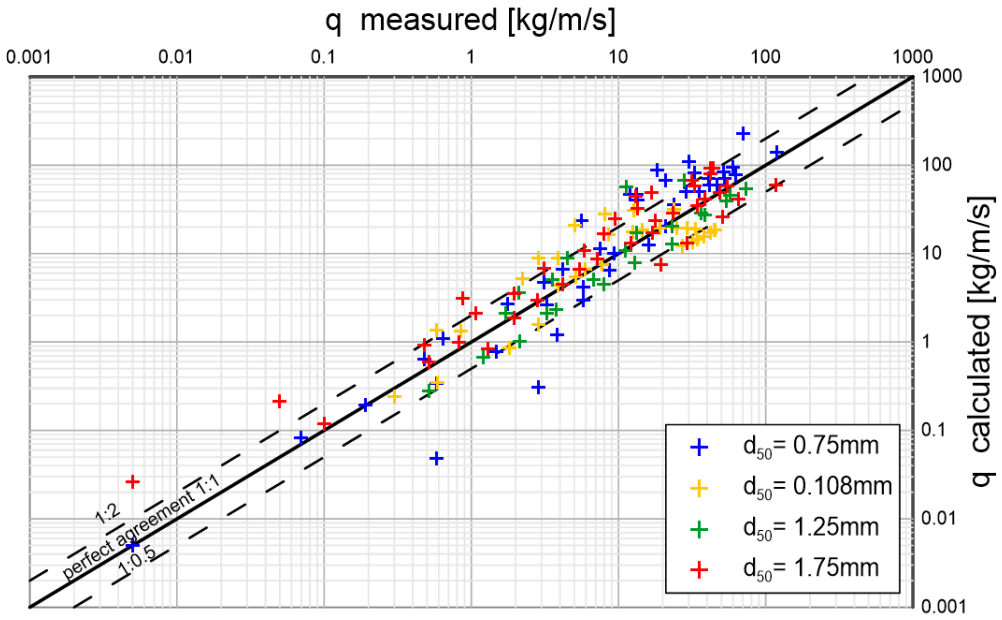

Figure 19. Measurement results of Larionov et al. [37] in relation to sediment transport values calculated with the presented three-layer model for four selected diameters in the range of variation in dimensionless friction $\Theta'_* = 0.06 \div 4$ under conditions of bottom slopes from 0.5% to 35%.

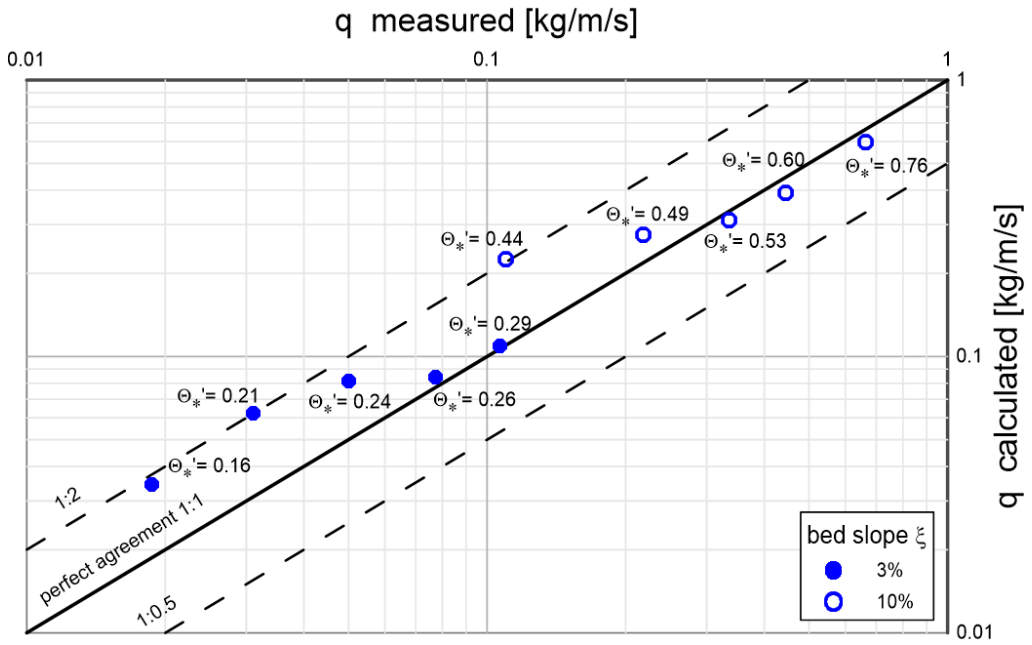

Figure 20. Comparison of example results of Aziz and Scott [38] measurements of 0.5mm diameter sediment transport intensity for two different bottom slopes: 3% (black dots) and 10% (circles) in the dimensionless friction range $\Theta'_* = 0.16 \div 0.76$ with the results of three-layer model calculations.

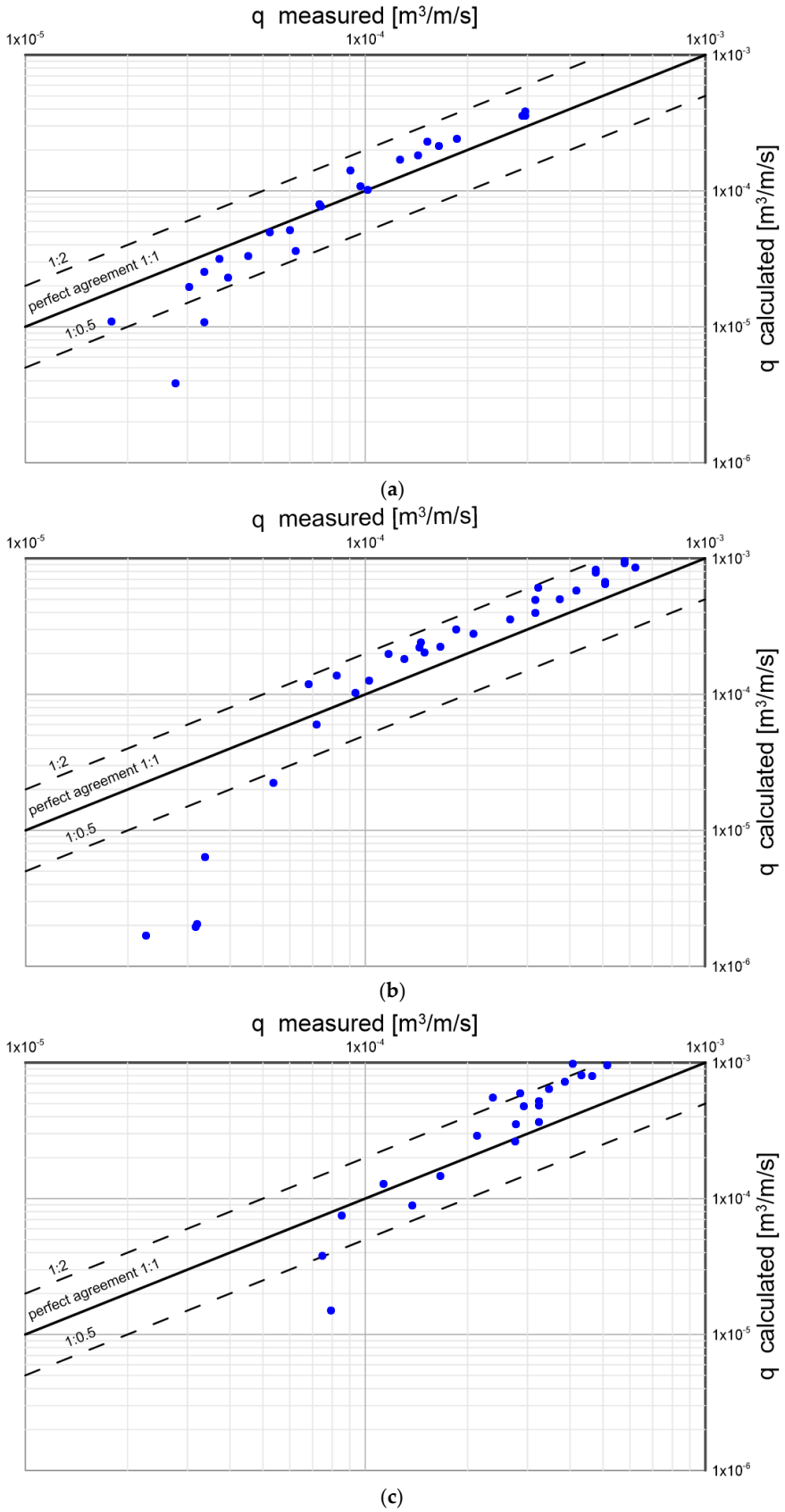

Figure 21. Comparison of values of sediment transport for three diameters under conditions of slopes from 0% to 10% in the range of dimensionless friction $\Theta'_* = 0.06 \div 0.29$ with the results of calculations with the multilayer model measured by Recking et al. [11]: (**a**) $d = 2.3$ mm; (**b**) $d = 4.9$ mm; and (**c**) $d = 9$mm.

5. Conclusions

The paper presents an innovative three-layer model for the description of granular sediment transport over a mobile bed with a variable slope in a steady flow. The influence of gravity on sediment movement in the lower layer is discussed in detail, which is crucial for understanding the mechanisms of sediment grain movement in rivers and hydraulic channels. This influence is very often overlooked in previous studies. The presented model allows for describing the vertical structure of transport and segregation of non-cohesive and granulometrically heterogeneous sediments under steady flow conditions in an open channel over a bed locally inclined in line with or opposite to the direction of sediment movement, in the range from zero to slopes close to the value of internal friction angle. Therefore, the proposed model enables us to better understand and predict sediment behavior, which is crucial in the context of hydrotechnical infrastructure design and water resources management.

The model based on the three-layer structure of sediment transport allows for a very detailed description of sediment behavior under different flow conditions. The paper identifies three main layers: bottom, contact, and upper layers, each with different characteristics of sediment transport and concentration. This segmentation allows for a better analysis and understanding of the interactions between the layers, which is fundamental for accurate modelling of natural processes.

The authors particularly emphasize the role of gravity in sediment transport in the lower layer (dense layer). Gravity has the effect of loosening the bottom and increasing the thickness of the lower layer and thus increasing the velocity at the upper boundary of this layer, which significantly affects the distribution of velocity and sediment concentration in the layers above. Understanding this mechanism is important for understanding the role of gravitational forces in sediment transport.

In this study, sediment transport over a bed with different slopes, from flat to slopes close to the angle of internal friction of the sediment, was modelled. The results of sediment transport modelling were compared with the results of experimental studies, obtaining a concordance of the results within double determination error.

In conclusion, the model presented in the paper offers an advanced tool for analyzing and predicting sediment behavior under varying hydraulic and morphological conditions.

Successful validation of the model for a very wide range of empirical data, including different slope types, grain diameters, densities, and grain mobility conditions, provides a strong basis for applying the model to real engineering conditions. The model has the potential to support decisions on water resources management, optimization of water infrastructure operation, and minimization of risks associated with erosion and material deposition in river and reservoir systems. Thus, the model's application in engineering practice can lead to significant improvements in the design of hydraulic infrastructure, such as dams, barrages, bridges, and irrigation and flood control systems.

Author Contributions: Conceptualization, L.M.K., J.B., M.P. and I.R.; methodology, L.M.K. and J.B.; formal analysis, L.M.K., J.B., M.P. and I.R.; investigation, L.M.K., J.B., M.P. and I.R.; resources, L.M.K., J.B., M.P. and I.R.; writing—original draft preparation, L.M.K., J.B., M.P. and I.R.; writing—review and editing, L.M.K., J.B., M.P. and I.R.; supervision, L.M.K.; project administration, J.B., M.P. and I.R.; funding acquisition, L.M.K., J.B., M.P. and I.R. All authors have read and agreed to the published version of the manuscript.

Funding: The research was financially supported by the research project of the Koszalin University of Technology, Faculty of Civil Engineering, Environmental and Geodetic Sciences: Dynamika niespoistego, niejednorodnego granulometrycznie ośrodka gruntowego w przepływie stacjonarnym i ruchu falowym w warunkach silnie nachylonego dna—funds no.: 524.01.07; project manager: L.K.

Data Availability Statement: The data presented in this study are available upon request from the corresponding author.

Conflicts of Interest: The authors declare no conflict of interest.

References

1. Lai, Y.G.; Huang, J.; Greimann, B.P. Hydraulic Flushing of Sediment in Reservoirs: Best Practices of Numerical Modeling. *Fluids* **2024**, *9*, 38. [CrossRef]
2. Shmakova, M. Sediment Transport in River Flows: New Approaches and Formulas. In *Modeling of Sediment Transport*; IntechOpen: London, UK, 2022. [CrossRef]
3. Andualem, T.G.; Hewa, G.A.; Myers, B.R.; Peters, S.; Boland, J. Erosion and Sediment Transport Modeling: A Systematic Review. *Land* **2023**, *12*, 1396. [CrossRef]
4. Berzi, D.; Fraccarollo, L. Intense sediment transport: Collisional to turbulent suspension. *Phys. Fluids* **2016**, *28*, 0233302. [CrossRef]
5. Meyer-Peter, E.; Müller, R. Formulas for bed-load transport. In Proceedings of the 2nd Meeting of the Int. Association for Hydraulic Structures Research, Delft, The Netherlands, 7 June 1948; International Association for Hydro-Environment Engineering and Research: Delft, The Netherlands, 1948.
6. Shields, A. *Anwendung der Aehnlichkeitsmechanik und der Turbulenzforschung auf die Geschiebebewegung*; Erschienen im Eigenverlag der Preussischen Versuchsanstalt für Wasserbau und Schiffbau: Berlin, Germany, 1936.
7. Smart, G.M. Sediment transport formula for steep channels. *J. Hydraul. Eng.* **1984**, *110*, 267–276. [CrossRef]
8. Wong, M.; Parker, G. Reanalysis and correction of bed-load relation of meyer-peter and müller using their own database. *J. Hydraul. Eng.* **2006**, *132*, 1159–1168. [CrossRef]
9. Cheng, N.-S.; Chen, X. Slope Correction for Calculation of Bedload Sediment Transport Rates in Steep Channels. *J. Hydraul. Eng.* **2014**, *140*. [CrossRef]
10. Graf, W.H.; Suszka, L. Sediment Transport in Steep Channels. *J. Hydrosci. Hydraul. Eng.* **1984**, *110*, 11–26. [CrossRef]
11. Recking, A.; Frey, P.; Paquier, A.; Belleudy, P.; Champagne, J.Y. Bed-load transport flume experiments on steep slopes. *J. Hydraul. Eng.* **2008**, *134*, 1302–1310. [CrossRef]
12. Parker, C.; Clifford, N.J.; Thorne, C.R. Understanding the influence of slope on the threshold of coarse grain motion: Revisiting critical stream power. *Geomorphology* **2011**, *126*, 51–65. [CrossRef]
13. Maurin, R.; Chauchat, J.; Frey, P. Revisiting slope influence in turbulent bedload transport: Consequences for vertical flow structure and transport rate scaling. *J. Fluid Mech.* **2018**, *839*, 135–156. [CrossRef]
14. Lamb, M.P.; Dietrich, W.E.; Venditti, J.G. Is the critical Shields stress for incipient sediment motion dependent on channel-bed slope? *J. Geophys. Res.* **2008**, *113*. [CrossRef]
15. Dang, T.A.; Park, S.D. Experimental Analysis and Numerical Simulation of Bed Elevation Change in Mountain rivers. *SpringerPlus* **2016**, *5*, 1075. [CrossRef] [PubMed]
16. António, S.D.; van der Werf, J.; Horstman, E.; Cáceres, I.; Alsina, J.; van der Zanden, J.; Hulscher, S. Influence of Beach Slope on Morphological Changes and Sediment Transport under Irregular Waves. *J. Mar. Sci. Eng.* **2023**, *11*, 2244. [CrossRef]
17. Qu, L.; Lei, T.; Zhou, C.; Yang, X. Measuring Sediment Transport Capacity of Concentrated Flow with Erosion Feeding Method. *Land* **2023**, *12*, 411. [CrossRef]
18. Yuan, J.; Tan, W. Modeling net sheet-flow sediment transport rate under skewed and asymmetric oscillatory flows over a sloping bed. *Coast. Eng.* **2018**, *136*, 65–80. [CrossRef]
19. Tan, W.; Yuan, J. Experimental study of sheet-flow sediment transport under nonlinear oscillatory flow over a sloping bed. *Coast. Eng.* **2019**, *147*, 1–11. [CrossRef]
20. Tan, W.; Yuan, J. Net sheet-flow sediment transport rate: Additivity of wave propagation and nonlinear waveshape effects. *Cont. Shelf Res.* **2020**, *240*, 104724. [CrossRef]
21. Radosz, I.; Zawisza, J.; Biegowski, J.; Paprota, M.; Majewski, D.; Kaczmarek, L.M. An Experimental Study on Progressive and Reverse Fluxes of Sediments with Fine Fractions in the Wave Motion over Sloped Bed. *Water* **2023**, *15*, 125. [CrossRef]
22. Radosz, I.; Zawisza, J.; Biegowski, J.; Paprota, M.; Majewski, D.; Kaczmarek, L.M. An Experimental Study on Progressive and Reverse Fluxes of Sediments with Fine Fractions in Wave Motion. *Water* **2022**, *14*, 2397. [CrossRef]
23. Kaczmarek, L.M.; Sawczyński, S.; Biegowski, J. An Equilibrium transport formula for modeling sedimentation of dredged channels. *Coast. Eng. J.* **2017**, *59*, 1750015-1–1750015-35. [CrossRef]
24. Kaczmarek, L.M.; Biegowski, J.; Sobczak, Ł. Modeling of Sediment Transport with a Mobile Mixed-Sand Bed in Wave Motion. *J. Hydraul. Eng.* **2022**, *148*, 04021054. [CrossRef]
25. Kaczmarek, L.M.; Ostrowski, R. Modelling of a three-layer sediment transport system in oscillatory flow. In Proceedings of the 26th International Conference on Coastal Engineering, Copenhagen, Denmark, 22–26 June 1998; pp. 2559–2572.
26. Kaczmarek, L.M.; Biegowski, J.; Sobczak, Ł. Modeling of Sediment Transport in Steady Flow over Mobile Granular Bed. *J. Hydraul. Eng.* **2019**, *145*, 04019009. [CrossRef]
27. Zawisza, J.; Radosz, I.; Biegowski, J.; Kaczmarek, L.M. Transport of Sediment Mixtures in Steady Flow with an Extra Contribution of Their Finest Fractions: Laboratory Tests and Modeling. *Water* **2023**, *15*, 832. [CrossRef]
28. Zawisza, J.; Radosz, I.; Biegowski, J.; Kaczmarek, L.M. Sand Transport with Cohesive Admixtures. . .—Laboratory Tests and Modeling. *Water* **2023**, *15*, 804. [CrossRef]
29. Cowen, E.A.; Dudley, R.D.; Liao, Q.; Variano, E.A.; Liu, P.L.-F. An insitu borescopic quantitative imaging profiler for the measurement of high concentration sediment velocity. *Exp. Fluids* **2010**, *49*, 77–88. [CrossRef]
30. Kaczmarek, L.M.; Zawisza, J.; Radosz, I.; Pietrzak, M.; Biegowski, J. The Application of Sand Transport with Cohesive Admixtures Model for Predicting Flushing Flows in Channels. *Water* **2024**, *16*, 1214. [CrossRef]

31. Sobczak, Ł. Dynamics of Grain-Inhomogeneous Sediment under Flow Conditions with a Moving Layer of an Inclined Bottom. Ph.D. Thesis, IBW PAN, Gdańsk, Poland, 2022. Available online: http://www.ibwpan.gda.pl/storage/app/media/doktoraty/doktorat_sobczak_rozprawa.pdf (accessed on 21 May 2023).
32. Sayed, M.; Savage, S.B. Rapid gravity flow of cohesionless granular materials down inclined chutes. *J. Appl. Math. Phys.* **1983**, *34*, 84–100. [CrossRef]
33. Frey, P. Particle velocity and concentration profiles in bedload experiments on a steep slope. *Earth Surf. Process. Landforms* **2014**, *39*, 646–655. [CrossRef]
34. Damgaard, J.; Soulsby, R.; Peet, A.; Wright, S. Sand transport on steeply sloping plane and rippled beds. *J. Hydraul. Eng.* **2003**, *129*, 706–719. [CrossRef]
35. Luque, R.F.; Van Beek, R. Erosion and transport of bed-load sediment. *J. Hydraul. Res.* **1976**, *14*, 127–144. [CrossRef]
36. Smart, G.M.; Jaeggi, M.N.R. Sediment transport on steep slopes. In *Mitteil. 64, Versuchsanstalt für Wasserbau, Hydrologie und Glaziologie*; ETH-Zürich: Zürich, Switzerland, 1983; p. 191.
37. Larionov, G.A.; Krasnov, S.F.; Dobrovol'skaya, N.G.; Kiryukhina, Z.P.; Litvin, L.F.; Bushueva, O.G. Equation of Sediment Transport for Slope Flows. *Eurasian Soil Sci.* **2006**, *39*, 868–878. [CrossRef]
38. Aziz, N.M.; Scott, D.E. Experiments on sediment transport in shallow flows in high gradient channels. *Hydrol. Sci.* **1989**, *34*, 465–478. [CrossRef]